

Robust underwater obstacle detection and collision avoidance

Varadarajan Ganesan¹ · Mandar Chitre¹ · Edmund Brekke²

Received: 8 December 2014 / Accepted: 9 December 2015
© Springer Science+Business Media New York 2015

Abstract A robust obstacle detection and avoidance system is essential for long term autonomy of autonomous underwater vehicles (AUVs). Forward looking sonars are usually used to detect and localize obstacles. However, high amounts of background noise and clutter present in underwater environments makes it difficult to detect obstacles reliably. Moreover, lack of GPS signals in underwater environments leads to poor localization of the AUV. This translates to uncertainty in the position of the obstacle relative to a global frame of reference. We propose an obstacle detection and avoidance algorithm for AUVs which differs from existing techniques in two aspects. First, we use a local occupancy grid that is attached to the body frame of the AUV, and not to the global frame in order to localize the obstacle accurately with respect to the AUV alone. Second, our technique adopts a probabilistic framework which makes use of probabilities of detection and false alarm to deal with the high amounts of noise and clutter present in the sonar data. This local probabilistic occupancy grid is used to extract potential obstacles which are then sent to the command and control (C2) system of the AUV. The C2 system checks for possible collision and carries out an evasive maneuver accordingly. Experiments are carried out to show the viability of the proposed algorithm.

Keywords Obstacle Detection · Collision Avoidance · Local Occupancy Grids

1 Introduction

In recent years, we have seen an increasing interest in autonomous underwater navigation and exploration. Although significant advances have been made in the development of autonomous underwater vehicles (AUVs), the technology for effective obstacle avoidance remains relatively immature. To carry out any long autonomous mission, the AUV's obstacle detection and avoidance system needs to be robust and capable of functioning in dynamic and highly uncertain environments. The absence of a robust obstacle detection and avoidance system can jeopardize the safety of an AUV during autonomous underwater missions. The obstacle detection system is in charge of analyzing scan lines from the sonar and detecting obstacles in the vicinity of the robot reliably. Once the obstacles have been detected, they are sent to the command and control (C2) system of the AUV to take action. The C2 system analyzes the detected obstacles and checks for potential collision between the AUV and the obstacles. If the C2 system expects a possible collision, it alters its path accordingly to ensure safe execution of the mission.

Multibeam and sector scanning forward looking sonars (FLS) are usually used for the purpose of obstacle detection. Although multibeam FLS are widely used in underwater environments for obstacle detection and avoidance due to their superior performance, they are usually more expensive than sector scanning sonars. Also, a typical multibeam sonar is larger in size compared to a sector scanning sonar and mounting it on AUVs where space is a constraint can be difficult. Our aim is to develop an algorithm for reliable obstacle detection that may be used with either type of FLS. We

✉ Varadarajan Ganesan
varadarajan@arl.nus.edu.sg

Mandar Chitre
mandar@arl.nus.edu.sg

Edmund Brekke
edmund.brekke@itk.ntnu.no

¹ Acoustic Research Laboratory, Tropical Marine Science Institute, Department of Electrical and Computer Engineering, National University of Singapore, Singapore, Singapore

² Department of Engineering Cybernetics, Norwegian University of Science and Technology, Trondheim, Norway

demonstrate our algorithm experimentally using data from the more challenging of the two, i.e., the sector-scanning sonar.

GPS signals are usually unavailable in underwater environments. Hence, AUVs generally rely on on-board proprioceptive sensors such as compass, doppler velocity log (DVL) and inertial navigation system (INS) for underwater positioning and navigation. Dead-reckoning using these sensors suffers from unbounded positioning error growth (Teck and Chitre 2014), which in turn leads to inaccurate localization of potential obstacles. However, for the purpose of obstacle avoidance, it is imperative to be able to localize the obstacles accurately.

The above mentioned problem is even more acute in low-cost AUVs where the proprioceptive sensors have low accuracy. Traditionally, this problem of improving the positional accuracy of the AUV has been solved by deploying external aids such as acoustic beacons, or by using sensors of higher accuracy. But both solutions incur additional costs. An interesting alternative is to use simultaneous localization and mapping (SLAM) where the detected obstacles are used as landmarks to improve positioning (Thrun et al. 2005; Leedekerken et al. 2006). SLAM holds great promise in solving the navigation and obstacle avoidance problems together, but issues such as feature representation, data association and consistency are still undergoing active research (Brekke and Chitre 2013). In our opinion, SLAM is not particularly suited for underwater obstacle detection and avoidance.

Furthermore, detection of targets is particularly difficult in underwater environments due to large amounts of background noise or clutter. Hence, one can expect a lot of false alarms (either due to noise or clutter) to be present in the scans received. With multibeam sonars, the traditional approach to dealing with false alarms is to use image processing techniques like segmentation and feature extraction from scan to scan to differentiate between potential targets and false alarms. However, the downside of using image processing methods are that they rely on some form of feature extraction technique which is not particularly reliable in underwater environments due to lack of distinct features.

The development of an obstacle detection and avoidance system that is insensitive to positional error growth and capable of dealing with a lot of false alarms will allow AUVs to run long autonomous missions. Collisions with obstacles that can otherwise jeopardize the safety of the AUV can be avoided. Hence, a robust obstacle detection and avoidance system ensures the safety of the AUV which is a fundamental requirement for achieving long term autonomy in underwater environments.

We propose an approach for detection and avoidance of obstacles which makes use of an occupancy grid that is attached to the AUV's body frame. Although occupancy grid formulations are common in land-based robotics (Elfes

1989; Konolige 1997; Thrun et al. 2005; Eliazar 2005), this approach is less popular in underwater robotics, some examples of which are presented in the works of Hernández et al. (2009) and Jakuba and Yoerger (2008).

Our proposed approach entails several novelties. As opposed to the more conventional geo-referenced occupancy grid, we use a *local occupancy grid* in the AUV's frame of reference. This is similar to the concept of robocentric SLAM (Castellanos et al. 2007). The reason for adopting this approach is that it is sufficient if the obstacles are accurately localized *relative* to the AUV for the purpose of obstacle avoidance alone. Accurate localization of obstacles in a geo-referenced frame is not required for avoidance, hence rendering a comprehensive mapping approach unnecessary. Adopting the AUV's body frame for obstacle localization makes the obstacle detection and avoidance performance insensitive to the AUV's positioning error growth.

Also, our formulation takes into account the motion uncertainties, and incorporates parameters such as false alarm rate and detection probability in a Bayesian framework to deal with the high amounts of false alarm present in the sonar data. As the AUV moves, the obstacles "move" with respect to the AUV in a manner relative to the motion of the AUV. We use a *motion model* which updates the probabilities of occupancy based on the estimated translational and rotational motion. When a sonar measurement becomes available, the occupancy probabilities are updated using a Bayesian *measurement model*. It integrates the new information from the sonar measurement into the belief map represented by the occupancy grid. The occupancy grid is used to determine the location of nearby obstacles. If these obstacles pose a threat of collision, the AUV's C2 system takes evasive maneuvers.

The main contributions of the work presented in this paper are as follows:

- Mathematical formulation of measurement and motion model for a local occupancy grid to deal with positional error growth of AUVs.
- Extension of the traditional occupancy grid formulation to include sensor parameters like probability of detection and false alarm.
- Validation of theoretical models for detection in background noise using experimental data.
- Experimental demonstration of obstacle detection and avoidance using an AUV equipped with a sector scanning sonar in lake and sea environments.

2 Related work

Developing an underwater obstacle detection and avoidance mechanism for an autonomous and remotely operated underwater robotic system is a challenging task for researchers. In

order to satisfy requirements for long term autonomy, the system needs to be robust and capable of handling uncertainties that are likely to arise during an underwater mission.

Over the years, many obstacle detection and avoidance techniques have been designed and implemented on autonomous underwater, ground and aerial robotic systems. All these works deal with two important requirements that are necessary for successful obstacle detection and avoidance. The first is the ability to detect obstacles from false alarms accurately and consistently. The second is to be able to accurately localize the obstacle in a frame of reference in order to execute safe avoidance maneuvers. While Sect. 2.1 deals with the former, Sects. 2.2 and 2.3 discuss works that tackle the latter issue. Additionally, Sect. 2.4 discusses works that address both the issues together.

2.1 Image processing techniques

Underwater robots use sonar based sensors for the purpose of detection in underwater environments. Typical scans received from these sensors have high amounts of false alarm present in them. Researchers have used image processing techniques like segmentation and feature extraction on these scans to distinguish obstacles from false alarm (Quidu et al. 2007; Teo et al. 2009; Tena Ruiz et al. 1999; Horner et al. 2005).

The authors in Zhao et al. (2009) used a sector scanning sonar to collect a sequential set of scan lines to create an image. Image processing techniques were then applied on this image. It should be noted that an image created by collecting scan lines over the entire sector as the AUV moves would not be accurate. Some form of motion compensation needs to be applied on the individual scan lines to create an accurate image. Furthermore, such an approach reduces the real time nature of the detection procedure.

Elsewhere, the authors in Quidu et al. (2007) and Teo et al. (2009) use a multibeam sonar to detect obstacles and avoid them. Here, instead of receiving a single scan line from a particular bearing, a complete scan over the entire sector is obtained. As a result, image processing techniques are applied on the scans received. In literature, it can be observed that the majority of obstacle detection and avoidance algorithms developed for mobile underwater robots use image processing techniques. These techniques have demonstrated reliability and extendability from a sector scanning sonar to a multibeam sonar. However, the authors in Tena Ruiz et al. (1999) acknowledge that the image processing techniques used in their work is computationally expensive and the scans were processed offline instead. Quidu et al. (2007) have also developed algorithms for offline processing of the data. Some image processing techniques use feature extraction methods to detect obstacles (Teo et al. 2009; Horner et al. 2005; Tena Ruiz et al. 1999). However, it is often very

difficult to extract reliable features from underwater environments using FLS data, especially when a sector scanning sonar is used.

2.2 SLAM techniques

Underwater robots also face the problem of localizing themselves since GPS signals are not available underwater. Hence, they suffer an unbounded positional error growth. As a result, detected obstacles cannot be localized accurately with respect to the global frame because of the existing positional error of the AUV. Researchers have used SLAM based techniques to reduce the positional error growth of the robot which in turn reduces the positional error of the obstacle. The authors in Leedekerken et al. (2006) use an extended Kalman Filter (EKF) as the main tool to carry out SLAM.

Feature extraction forms a key component of some SLAM based techniques (Ribas et al. 2008; Majumder et al. 2001). In Majumder et al. (2001), the authors fuse data from sonar and vision sensors, following which feature extraction is performed on the fused data. The posterior distribution of the map is updated using a Bayesian approach for each identified feature. However, successful extraction of features is only possible if the features are distinct and can be associated with some form of geometrical representation (e.g., walls can be represented by straight lines). Underwater environments generally lack such features and hence map building using feature extraction techniques may not be a reliable approach.

SLAM holds great promise in solving the navigation and obstacle avoidance problems together, but issues such as feature representation, data association and consistency are still undergoing active research.

2.3 Scan matching techniques

Another interesting strategy adopted by researchers to minimize the positioning error is to register the overlap between two consecutive scans (scan matching) and hence correct the estimated dead-reckoned displacement (Hurtós et al. 2015; Burguera et al. 2012). While SLAM techniques rely on features for reliable performance, scan matching techniques can work with featureless data. However, issues such as data association and consistency, which exist in SLAM techniques, do persist in scan matching as well. Furthermore, there still exists a drift in the position of the AUV which increases with time, as can be seen in Burguera et al. (2012) and Hernández et al. (2009).

2.4 Occupancy grids

Occupancy grids are better equipped to deal with noisy data since they associate a probability of occupancy to every cell

on the grid instead of using a hard threshold on the intensity value to indicate a detection.

There are two types of occupancy grids that can be used for the purpose of obstacle detection and navigation. They are:

1. A *global occupancy grid* which is used to create a comprehensive map of all the detected features and obstacles in a global frame of reference. Robots that create a global occupancy grid need to account for their increasing positional uncertainty while adding detected obstacles and features.
2. A *local occupancy grid* which is attached to the robot's body frame and adds obstacles detected in the vicinity of the robot. When the robots moves, the obstacles (static) "move" in the local occupancy grid in a manner relative to the motion of the robot. Obstacles are localized accurately with respect to the AUV, a method which is sufficient for the purpose of avoidance.

In [Elfes \(1989\)](#) and [Konolige \(1997\)](#), the authors provide a mathematical formulation to generate a global occupancy grid using sonar data for the purpose of navigation while taking into account the increasing error in the position of the robot. Local occupancy grids have also been used for the purpose of navigation and obstacle avoidance. The authors in [Fulgenzi et al. \(2007\)](#) and [Marlow and Langelaan \(2010\)](#) used the same to navigate safely in the presence of obstacles in land and aerial environments respectively.

Occupancy grids have also been used in the underwater domain for various applications ([Fairfield et al. 2007](#); [Hernández et al. 2009](#); [Jakuba and Yoerger 2008](#)). The authors in [Fairfield et al. \(2007\)](#) have formulated a particle filter based SLAM where each particle uses an occupancy grid based representation of the world in order to circumvent the problem of feature extraction. In [Hernández et al. \(2009\)](#) and [Jakuba and Yoerger \(2008\)](#), the authors have used occupancy grids for mapping purposes and for searching hydrothermal vent fields respectively.

Finally, in [Martin et al. \(2000\)](#) and [Chew and Chitre \(2013\)](#), the authors present results of obstacle detection using occupancy grids in a controlled environment and under static conditions. In [Horner et al. \(2009\)](#), the authors use forward looking sonars in the vertical and horizontal directions to build a 3D global occupancy grid which they use for navigation purposes. While they take background noise distribution and obstacle detection model into account, they incorporate them into their Bayesian framework in a look-up table manner as opposed to our approach which makes use of a formal sonar detection theory. Furthermore, to the best of our knowledge, there has been no experimental results showing obstacle detection and avoidance with the AUV in a dynamic

state using local occupancy grids in an underwater environment.

3 Technical approach

We use a local occupancy grid to represent our belief of the location of nearby obstacles. We require a motion model and measurement model to update the occupancy grid as the AUV moves and whenever sonar measurements become available. Finally, we require a detection procedure that operates on the occupancy grid to yield a set of potential obstacles. This set of potential obstacles is sent to the AUV's C2 system to check for collision, and to plan evasive maneuvers if necessary.

3.1 Background information

An FLS sends out a sonar "ping" in a given direction and listens for echoes. The echo intensity profile returned from the environment is discretized into a set of bins (k, θ) where index k represents the range, and index θ represents the bearing. Let the measurement observed in bin (k, θ) be $z_{k,\theta}$. Given a threshold value t_k for range bin k , we report a detection $S_{k,\theta} = 1$ if $z_{k,\theta} \geq t_k$ and $S_{k,\theta} = 0$ otherwise.

Let p_k be the probability of detection of an obstacle at a range corresponding to bin k , and f_k be the probability of false alarm, both of which are necessary operational parameters. p_k is indicative of the probability with which the measurement $z_{k,\theta}$ obtained ($> t_k$) is due to presence of a target. f_k is a measure of the probability with which the measurement $z_{k,\theta}$ is obtained ($> t_k$) when there is no target present, in other words due to clutter. A plot of p_k vs f_k (parametrized by t_k) is known as the receiver operating characteristic (ROC) curve. This ROC curve varies with signal-to-noise ratio (SNR) and environmental characteristics; we can experimentally measure this for a sonar in an operational environment of interest.

Hence, p_k and f_k varies as t_k varies. We set a constant acceptable false alarm rate f (i.e., set $f_k = f$) and obtain the corresponding p_k and t_k for each range bin k .

3.2 Local occupancy grid

The local occupancy grid is defined such that it is rectangular with $m \times n$ occupancy cells. The size of an occupancy cell is $l \times l$ and each one is at a fixed location with respect to the AUV. An illustration of the local occupancy grid and the sensor frame (dark blue color) attached to the AUV is shown in [Fig. 1](#). Occupancy cell with index (x, y) is denoted by $O_{x,y}$. Accordingly, each occupancy cell $O_{x,y}$ is associated with the events $\mathbb{O}_{x,y}$ that it is occupied, and $\overline{\mathbb{O}}_{x,y}$ that it is not occupied. The probability with which an occupancy cell $O_{x,y}$

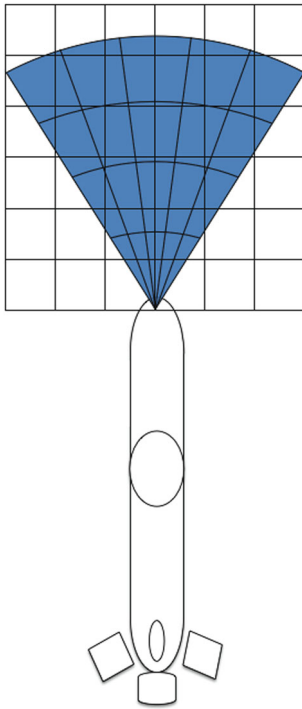


Fig. 1 Illustration of local occupancy grid attached to the AUV and its sensor frame (dark blue color) (Color figure online)

is occupied is denoted by $P(\mathbb{O}_{x,y})$. Therefore, the two events are related such that $P(\mathbb{O}_{x,y}) + P(\widehat{\mathbb{O}_{x,y}}) = 1$. The $m \times n$ matrix, \mathbf{P} , of occupancy probabilities [$P(\mathbb{O}_{x,y}) \forall x, y$] fully describes the belief held by the algorithm about obstacles in the vicinity of the AUV.

3.2.1 Measurement model

The occupancy grid serves as a Bayesian prior and is updated when a measurement is available. The probabilities p_k and f , and Bayes' rule are used to update the occupancy cells to their posterior probabilities. The manner in which the cells are updated depends on whether $S_{k,\theta} = 1$ ($z_{k,\theta} \geq t_k$) or $S_{k,\theta} = 0$ ($z_{k,\theta} < t_k$).

Let $O_{k,\theta}^{x,y}$ denote the region of overlap between range bin (k, θ) and any occupancy cell $O_{x,y}$. Accordingly, let the event that the region $O_{k,\theta}^{x,y}$ is occupied be denoted by $\mathbb{O}_{k,\theta}^{x,y}$. Our measurement model is defined such that $S_{k,\theta} = 1$ will be observed when a target is present in any one of the overlapping regions $O_{k,\theta}^{x,y}$ with a probability equal to the probability of detection. Hence, four possible combination of events are possible. They are:

$$P(S_{k,\theta} = 1 | \mathbb{O}_{k,\theta}^{x,y}) = p_k \tag{1}$$

$$P(S_{k,\theta} = 1 | \widehat{\mathbb{O}_{k,\theta}^{x,y}}) = f \tag{2}$$

$$P(S_{k,\theta} = 0 | \mathbb{O}_{k,\theta}^{x,y}) = 1 - p_k \tag{3}$$

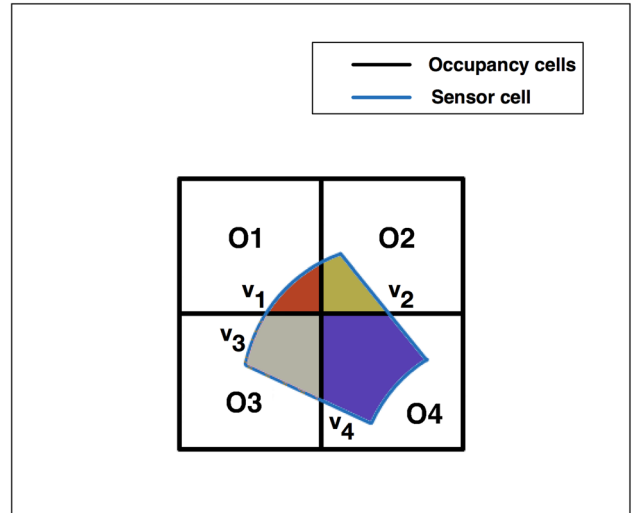


Fig. 2 Illustration of overlap between occupancy cells and a sensor cell. The area of overlap between a range bin and $O\{i\}$, is $v_{\{i\}}$ where $i \in \{1, \dots, 4\}$

$$P(S_{k,\theta} = 0 | \widehat{\mathbb{O}_{k,\theta}^{x,y}}) = 1 - f \tag{4}$$

The overlap between occupancy cells and a particular range bin is shown in Fig. 2.

Let $v_{k,\theta}^{x,y}$ denote the area of overlap between range bin (k, θ) and occupancy cell $O_{x,y}$, and $A(O_{x,y})$ denote the area of an occupancy cell. Following this, the events $\mathbb{O}_{k,\theta}^{x,y}$ and $\mathbb{O}_{x,y}$ are related as follows:

$$P(\mathbb{O}_{k,\theta}^{x,y} | \mathbb{O}_{x,y}) = \frac{v_{k,\theta}^{x,y}}{A(O_{x,y})} = a_{k,\theta}^{x,y} \tag{5}$$

$$P(\widehat{\mathbb{O}_{k,\theta}^{x,y}} | \mathbb{O}_{x,y}) = 1 - a_{k,\theta}^{x,y} \tag{6}$$

$$P(\widehat{\mathbb{O}_{k,\theta}^{x,y}} | \widehat{\mathbb{O}_{x,y}}) = 1 \tag{7}$$

$$P(\mathbb{O}_{k,\theta}^{x,y} | \widehat{\mathbb{O}_{x,y}}) = 0 \tag{8}$$

Finally, the map is updated for the two possible cases corresponding to $S_{k,\theta} = 1$ or $S_{k,\theta} = 0$, as follows:

Case 1 When the measurement obtained is such that $S_{k,\theta} = 1$ ($z_{k,\theta} \geq t_k$), the occupancy cell $O_{x,y}$ is updated as:

$$P(\mathbb{O}_{x,y} | S_{k,\theta} = 1) = \frac{P(S_{k,\theta} = 1 | \mathbb{O}_{x,y})P(\mathbb{O}_{x,y})}{P(S_{k,\theta} = 1)} \tag{9}$$

$$P(S_{k,\theta} = 1 | \mathbb{O}_{x,y}) = 1 - P(S_{k,\theta} = 0 | \mathbb{O}_{x,y}) \tag{10}$$

$$P(S_{k,\theta} = 0 | \mathbb{O}_{x,y}) = \prod_{i=1}^m \prod_{j=1}^n \left\{ \sum_{\mathbb{O}_{i,j}} \sum_{\widehat{\mathbb{O}_{i,j}^{i,j}}} P(S_{k,\theta} = 0 | \mathbb{O}_{i,j}^{i,j}) \times P(\mathbb{O}_{k,\theta}^{i,j} | \mathbb{O}_{i,j}) P(\mathbb{O}_{i,j} | \mathbb{O}_{x,y}) \right\} \tag{11}$$

$$\begin{aligned}
&= \prod_{i=1}^m \prod_{j=1}^n \left\{ P(S_{k,\theta} = 0 | \mathbb{O}_{k,\theta}^{i,j}) P(\mathbb{O}_{k,\theta}^{i,j} | \mathbb{O}_{i,j}) P(\mathbb{O}_{i,j} | \mathbb{O}_{x,y}) \right. \\
&\quad + P(S_{k,\theta} = 0 | \widehat{\mathbb{O}}_{k,\theta}^{i,j}) P(\widehat{\mathbb{O}}_{k,\theta}^{i,j} | \mathbb{O}_{i,j}) P(\mathbb{O}_{i,j} | \mathbb{O}_{x,y}) \\
&\quad + P(S_{k,\theta} = 0 | \widehat{\mathbb{O}}_{k,\theta}^{i,j}) P(\widehat{\mathbb{O}}_{k,\theta}^{i,j} | \widehat{\mathbb{O}}_{i,j}) P(\widehat{\mathbb{O}}_{i,j} | \mathbb{O}_{x,y}) \\
&\quad \left. + P(S_{k,\theta} = 0 | \widehat{\mathbb{O}}_{k,\theta}^{i,j}) P(\widehat{\mathbb{O}}_{k,\theta}^{i,j} | \widehat{\mathbb{O}}_{i,j}) P(\widehat{\mathbb{O}}_{i,j} | \mathbb{O}_{x,y}) \right\} \quad (12)
\end{aligned}$$

$$\begin{aligned}
&= \left(1 - f + a_{k,\theta}^{x,y} (f - p_k) \right) \\
&\quad \times \left\{ \prod_{i=1}^m \prod_{j=1}^n \left\{ \left(1 - f + a_{k,\theta}^{i,j} (f - p_k) \right) P(\mathbb{O}_{i,j}) \right. \right. \\
&\quad \left. \left. + (1 - f) P(\widehat{\mathbb{O}}_{i,j}) \right\} \forall (i, j) \neq (x, y) \right\} \quad (13)
\end{aligned}$$

$$P(S_{k,\theta} = 1) = 1 - P(S_{k,\theta} = 0) \quad (14)$$

$$\begin{aligned}
P(S_{k,\theta} = 0) &= \prod_{i=1}^m \prod_{j=1}^n \left\{ \sum_{\mathbb{O}_{i,j} \mathbb{O}_{k,\theta}^{i,j}} \sum_{\mathbb{O}_{i,j} \widehat{\mathbb{O}}_{k,\theta}^{i,j}} P(S_{k,\theta} = 0 | \mathbb{O}_{k,\theta}^{i,j}) \right. \\
&\quad \left. \times P(\mathbb{O}_{k,\theta}^{i,j} | \mathbb{O}_{i,j}) P(\mathbb{O}_{i,j}) \right\} \quad (15)
\end{aligned}$$

$$\begin{aligned}
P(S_{k,\theta} = 0) &= \prod_{i=1}^m \prod_{j=1}^n \left\{ \left(1 - f + a_{k,\theta}^{i,j} (f - p_k) \right) \right. \\
&\quad \left. \times P(\mathbb{O}_{i,j}) + (1 - f) P(\widehat{\mathbb{O}}_{i,j}) \right\} \quad (16)
\end{aligned}$$

where the normalizing constant is given by $P(S_{k,\theta} = 1)$ and the likelihood of getting a measurement $S_{k,\theta} = 1$ ($z_{k,\theta} \geq t_k$) from range bin (k, θ) given $O_{x,y}$ is already occupied is denoted by $P(S_{k,\theta} = 1 | \mathbb{O}_{x,y})$. Note that $a_{k,\theta}^{i,j}$ equals zero when the occupancy cell is far away from the range bin (k, θ) . Because of this, it is sufficient to update the probabilities of a neighbourhood of $r \times r$ occupancy cells that enclose the range bin (k, θ) . Likewise, while updating a particular occupancy cell $O_{x,y}$ in the $r \times r$ neighbourhood, the occupancy cells $O_{i,j}$ in the same neighbourhood will only be involved.

It should be noted that $S_{k,\theta} = 0$ occurs only when a detection was missed or there was no target present in **all** the overlapping cells. Hence $P(S_{k,\theta} = 0)$ can be calculated in a simpler manner. But in the case when $S_{k,\theta} = 1$ occurs, all possible combination of detections and/or false alarms from all possible combination of overlapping occupancy cells need to be taken into account. Therefore, calculating $P(S_{k,\theta} = 1)$ becomes a rather convoluted process.

Case 2 When the measurement obtained is such that $S_{k,\theta} = 0$ ($z_{k,\theta} < t_k$), the occupancy cell $O_{x,y}$ is updated in a slightly different manner.

$$P(\mathbb{O}_{x,y} | S_{k,\theta} = 0) = \frac{P(S_{k,\theta} = 0 | \mathbb{O}_{x,y}) P(\mathbb{O}_{x,y})}{P(S_{k,\theta} = 0)} \quad (17)$$

where $P(S_{k,\theta} = 0)$ is the normalizing constant and can be obtained from Eqs. (15) and (16). $P(S_{k,\theta} = 0 | \mathbb{O}_{x,y})$ denotes the likelihood of getting a measurement $z_k < t_k$ from a range bin (k, θ) given $O_{x,y}$ is occupied and can be calculated as per Eq. (11).

The implicit assumption made in the formulation is the events that two occupancy cells are occupied are independent of each other, i.e. $P(\mathbb{O}_{i,j} | \mathbb{O}_{x,y}) = P(\mathbb{O}_{i,j})$. This is justified because an obstacle in one occupancy cell is not likely to contribute to a sonar measurement from another occupancy cell. While other occupancy grid based formulations use the assumption of independence to ensure that the calculation of probabilities do not become intractable, we use the assumption as a convenience. This is primarily because the update of a single occupancy cell would propagate through the entire map (Fairfield et al. 2007) and we control this propagation by taking into consideration the area of overlap of the range bin with the occupancy cells as mentioned above.

3.2.2 Motion model

The motion model accounts for the translational and the rotational motion of the AUV and updates the probabilities of the occupancy cells accordingly. We define our motion model such that the translational motion is decoupled from the rotational motion. Although translational and rotational motions happen simultaneously, decoupling both of them allows for real time performance of the detection algorithm. Justification of this approximation is detailed in Appendix 2.

Translational Motion The translational motion is modelled as a convolution between the cell probabilities and an appropriate kernel \mathbf{K} . The choice of kernel \mathbf{K} depends on whether the AUV undergoes deterministic or probabilistic motion.

Deterministic Motion Whenever GPS or DVL is available, it is reasonable to model the AUV's motion as deterministic due to the high accuracy of GPS signals and low process noise of the DVL. Additionally, GPS receivers have an inbuilt filter which tracks the position, and in the process reduces the error between readings which justifies the use of a deterministic model. In this case, the occupancy grid is simply shifted by the amount of displacement. An illustration of how the occupancy probability is updated through a convolution when the robot undergoes translational motion is shown in Fig. 3.

The kernel is chosen based on the amount of displacement the robot has undergone between two timesteps. In our case, the kernel is an $N \times N$ matrix. Figure 3 shows the elements of the kernel based on the amount of displacement undergone. The mathematical form of the motion update is as follows:

$$\mathbf{P}_t = \mathbf{P}_{t-1} \otimes \mathbf{K} \quad (18)$$

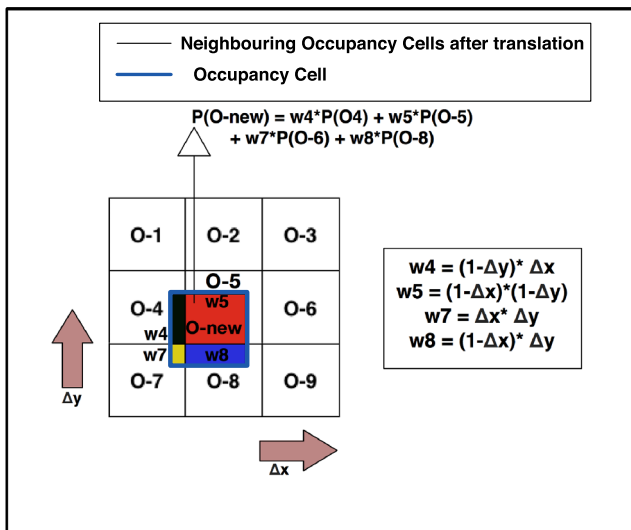


Fig. 3 Illustration of overlap of neighbouring occupancy cells after undergoing translation with a particular occupancy cell. The area of overlap between O-new and O-*i*, is $w_{\{i\}}$ where $i \in \{4, 5, 7 \text{ and } 8\}$. The size of each occupancy cell is 1 unit \times 1 unit

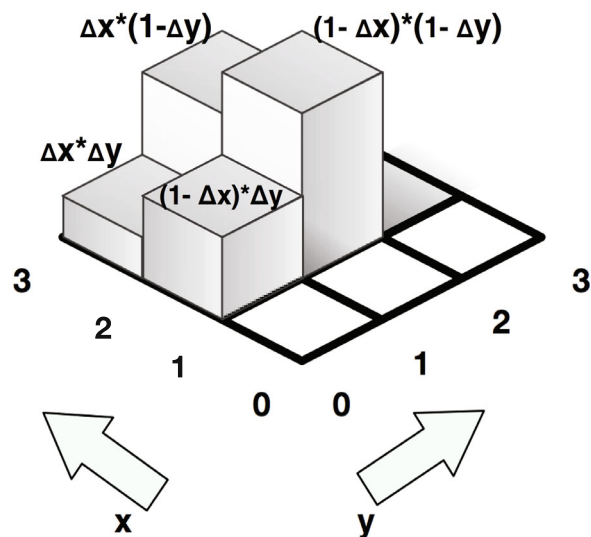
where \otimes is the convolution symbol and \mathbf{P}_{t-1} is the matrix representation of the entire occupancy grid at time $t - 1$. **Probabilistic Motion** In the absence of GPS signals and DVL measurements, the displacement is unimodal with its peak representing the mean translational motion, and the spread represents the uncertainty associated with the motion estimate. The uncertainty is modelled as a Gaussian distribution, denoted by $\mathcal{N}(\boldsymbol{\mu}, \mathbf{R})$ where $\boldsymbol{\mu}$ is the mean displacement of the AUV and variance, \mathbf{R} , is the process noise of the thruster model. A typical element for this type of kernel is as follows:

$$\mathbf{K}_{ij} = \iint_A \mathcal{N}(\boldsymbol{\mu}, \mathbf{R}) dx dy \tag{19}$$

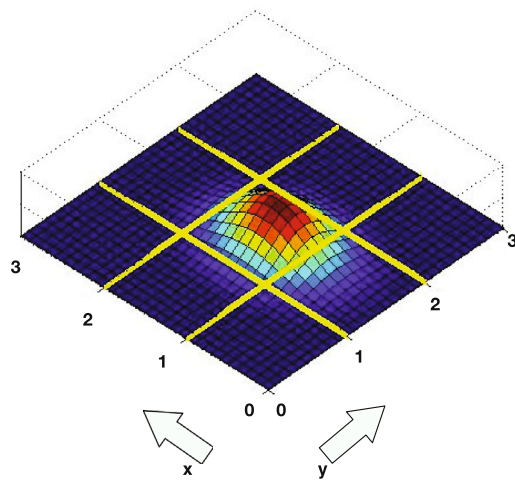
The integral is evaluated over the region of the distribution represented by the element \mathbf{K}_{ij} . The grid is then updated in accordance with Eq. (18). In this case, the process noise should be large enough such that the spread of the distribution is greater than the region represented by a single kernel element. If the process noise is low, the motion can be considered deterministic instead.

Graphical representations of typical kernels (3 \times 3 matrix) used in our work are shown in Fig. 4. While Fig. 4a shows the kernel used for convolution when the motion of the AUV is considered to be deterministic, Fig. 4b illustrates the kernel used when the displacement is uncertain. In Fig. 4b, it should be noted that volume under the region represented as grids by bold yellow lines gives the necessary elements of the kernel matrix in accordance with Eq. (19).

Rotational Motion The rotational motion of the AUV is modelled as deterministic in nature owing to the high accu-



(a)



(b)

Fig. 4 Graphical representation of Kernels. **a** Deterministic Kernel. **b** Probabilistic Kernel

racy of the compass being used. In order to avoid round off errors, changes in heading are accumulated until they reach $\pm 1^\circ$. Following this, the area of overlap of the neighbouring occupancy cells after rotation $O'_{x-i,y-j} \forall i, j \in \{-1, 0, 1\}$ with a particular occupancy cell $O_{x,y}$ is calculated as follows:

$$\Delta_{x,y}^{x-i,y-j} = \left| 0.5 \left\{ \sum_{k=1}^{n-1} (\bar{x}_k \bar{y}_{k+1} - \bar{y}_k \bar{x}_{k+1}) + (\bar{x}_n \bar{y}_1 - \bar{y}_n \bar{x}_1) \right\} \right| \tag{20}$$

where $(\bar{x}_k, \bar{y}_k) \forall k \in \{1, \dots, n\}$ are the coordinates of intersection between occupancy cell $O'_{x-i,y-j}$ and $O_{x,y}$. Then

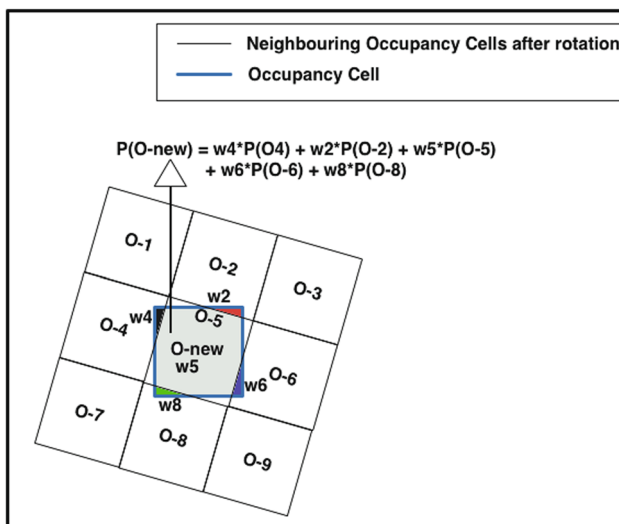


Fig. 5 Illustration of overlap of neighbouring occupancy cells after undergoing rotation with a particular occupancy cell. The area of overlap between O-new and O- $\{i\}$ is $w\{i\}$ where $i \in \{2, 4, 5, 6 \text{ and } 8\}$

the new probability of occupancy is updated as:

$$P(O_{x,y}) = \sum_i \sum_j w_{x,y}^{x-i,y-j} P(O'_{x-i,y-j}) \quad (21)$$

$$w_{x,y}^{x-i,y-j} = \frac{\Delta_{x,y}^{x-i,y-j}}{A(O_{x,y})} \quad (22)$$

where $A(O_{x,y})$ is the area of occupancy cell $O_{x,y}$. An illustration of how the probability is updated in the presence of rotation is shown in Fig. 5. Since the rotational update is performed only after the change in heading has accumulated till $\pm 1^\circ$, all values of $w_{x,y}^{x-i,y-j}$ throughout the grid are calculated offline and then used online. It should be noted that two sets of $w_{x,y}^{x-i,y-j}$ values need to be calculated; one for $+1^\circ$ change in heading and another for -1° change in heading.

3.3 Detection procedure

Let $N_{x,y}$ denote the expected number of obstacles in the neighbourhood of an occupancy cell $O_{x,y}$. It can be calculated as follows:

$$N_{x,y} = \sum_i \sum_j P(O_{x-i,y-j}) \quad \forall i, j \in \{-a, \dots, 0, \dots, a\}; i, j \in \mathbb{I} \quad (23)$$

We set a threshold P_{thresh} and declare a detected obstacle in the neighbourhood if $N_{x,y} \geq P_{\text{thresh}}$. At the end of every scan, the obstacles detected throughout the grid is sent to the command and control (C2) system of the AUV to carry out avoidance maneuvers if necessary.

The rationale behind using a neighbourhood to detect obstacles is that obstacles are not entirely confined to a particular occupancy cell. Moreover, the detection procedure is applied only at the end of every scan. As a result, obstacles may have moved relative to the AUV (since the AUV may be in motion) from the time they were actually seen. Hence the neighbourhood is defined such that the obstacle does not “move” beyond the boundary of the neighbourhood. In our work, we chose the neighbourhood to be 3×3 occupancy cells (i.e., $a = 1$);

3.4 Avoidance procedure

A local avoidance approach to obstacle avoidance has been adopted in our work. This is because the AUV executes an avoidance behavior as and when it sees an obstacle which poses a threat of collision.

The obstacle avoidance component is incorporated in the STARFISH AUV (Koay et al. 2011) within its C2 system (Teck and Chitre 2012). The C2 architecture used in the STARFISH AUV is based on a hybrid hierarchical control architecture. It adopts a deliberative-reactive architecture that consists of agents. The functions of some of the important agents are discussed below:

- Captain* Responsible for starting and coordinating missions.
- Executive Officer* Receives mission points from the Captain and sends them to the Navigator for planning waypoints. Mission points are user defined and are in the global frame of reference.
- Navigator* Plans waypoints (also in the global frame) to a mission point and sends them to the Executive Officer which again sends them to the Pilot.
- Pilot* Receives the waypoints from the Executive officer and executes them in a systematic manner by defining set-points for the vehicle parameters like bearing, speed, depth and altitude.

For the purpose of avoidance, the behavior of the following agents were modified in the C2 system:

3.4.1 FLS detector

This agent is newly added and directly communicates with the FLS and receives scan lines continuously from the sonar. It processes these scan lines according to the methods in Sect. 3.2 to generate a local occupancy grid. After this, an obstacle detection procedure (Sect. 3.3) is used at the end of a complete scan to detect likely obstacles in the vicinity of the AUV. This procedure creates a detection map in the AUV’s frame of reference. The detection map is then sent to

the Navigator of the AUV at the end of every scan for further actions.

3.4.2 Navigator

This default C2 agent was modified to include the functionality explained below. Once the Navigator receives a detection map from the FLSDetector, it creates a new map by providing a clearance radius to the obstacle. The clearance radius is defined such that o cells around the obstacle are marked as no-go zone. We refer to this new map as an obstacle map.

Since the obstacle map is in the local frame of the AUV, the waypoints being executed need to be transformed to the AUV's frame of reference to check for possible collision. Additionally, the positioning system of the AUV is not reliable as it is susceptible to drift during underwater missions. Hence, transforming the waypoints to the AUV's frame of reference also eliminates any uncertainty associated with the position of the AUV.

Once the waypoints to the mission point being executed are transformed into the AUV's frame of reference, the Navigator looks for possible collision between the waypoints and the obstacles in the detection map. The Navigator confirms the possibility of a collision if any one of the waypoints lies on the obstacle or if the line joining 2 waypoints intersects with the obstacle.

After detecting a collision, the Navigator immediately replans a new set of waypoints to the next mission point using an A* search algorithm (Hart et al. 1968). If the goal node (mission point) lies on an obstacle (no feasible path exists) or if there is an obstacle within 10 m radius of the goal node, the Navigator aborts that particular mission point. Instead, the goal node is set to the subsequent mission point and a new path is planned to that mission point. We take this approach to ensure the safety of the AUV. Also, the Captain is notified of such a modification to the mission plan. Other algorithms for path planning such as D* (Stentz 1994) can also be adopted by the Navigator.

These new waypoints are then transformed back to the global frame since they are required to be in the global frame in order to be executed by the Pilot. Although there might be errors in the waypoints when they are transformed back to the global frame, the same amount of error would be present in the position of the obstacle as well. As a result, the relative distance between the waypoints and the obstacle would be same even in the global frame of reference, which is sufficient for executing an avoidance maneuver. The idea of planning in the AUV's frame of reference makes the newly generated waypoints insensitive to the positional error associated with the AUV. Hence, the AUV can execute an avoidance maneuver safely even if there is an uncertainty associated with its position.

4 Results

4.1 Obstacle detection

Experiments were conducted at Pandan reservoir in Singapore and also in the sea off the coast of Singapore. For both sets of experiments, we used a Micron DST sector scanning sonar integrated on our STARFISH AUV (Koay et al. 2011). The sonar was configured for 50 m operating range with 44 bins and 90° scan sector.

During the Pandan experiment, the mission was planned such that the AUV was operating near some static buoys and the reservoir's embankments. The mission was executed with the AUV maintaining a constant depth of 0.5 m and at an altitude of 2–4 m from the lake bottom. Figure 6 shows the Micron DST sector scanning sonar mounted on the nose section of the STARFISH AUV before being deployed for a mission at Pandan reservoir. The mission path and the obstacles in the environment are shown in Fig. 7a. The lower embankment wall is not visible from the surface, but is instead marked in Fig. 7a using a dashed line. Figure 8 shows an illustration of the embankment at the reservoir.

The experiment at the sea was conducted at Selat Pauh, an anchorage area south of Singapore with a depth of 7–25 m. The AUV was tasked to run close to a shallow coral reef (<3 m). The mission was planned such that the AUV swam on the surface. The path taken by the AUV and the location of the shallow reefs are shown in Fig. 7b.

4.1.1 Noise distribution, ROC curves and operating p_k

FLS scans from the missions at Pandan reservoir and at Selat Pauh were processed offline to obtain the background noise distribution. This was achieved by analyzing scans obtained from the FLS when there was no obstacle in its field of view. At Pandan reservoir, the background noise was found to be



Fig. 6 STARFISH AUV

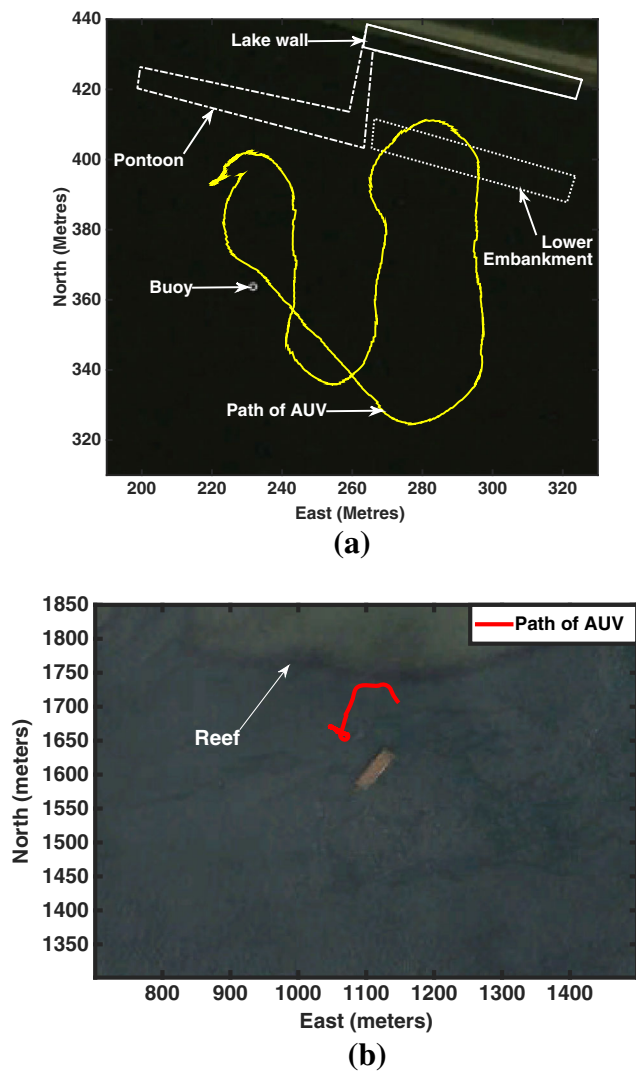


Fig. 7 Experiments at Pandan reservoir and at sea. **a** Path of the AUV and location of obstacles at Pandan reservoir. **b** Path of the AUV and location of the reef at sea

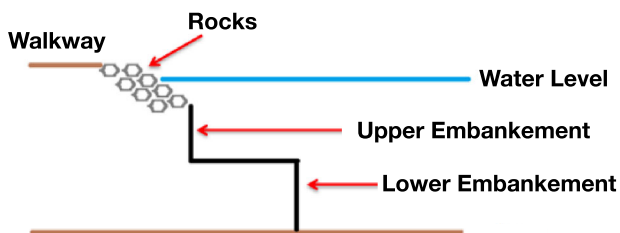


Fig. 8 Illustration showing the structure of embankments at Pandan reservoir

well described by a Gaussian distribution. Figure 9 shows the distribution of the background noise for different range bins and the corresponding Gaussian fit.

On the other hand, a stable distribution was found to better represent the distribution of the background noise at Selat

Pauh. Figure 10 shows the distribution of the background noise for different range bins and the corresponding stable fit. Stable distributions are typically used to describe impulsive noise which can be attributed to the presence of snapping shrimps which are usually found in warm shallow underwater environments (Chitre et al. 2006).

After marking the obstacles in the map (Fig. 7), we calculated the values of p_k and f_k offline by varying the threshold value, t_k , on the measurement $z_{k,\theta}$. The values of p_k and f_k are the frequencies of detection ($z_{k,\theta} > t_k$ when there was an obstacle present) and false alarm ($z_{k,\theta} > t_k$ when there was no obstacle present). The values of p_k and f_k can also be obtained online by performing a simple calibration experiment before running a mission. The experiment involves collecting scans from the FLS when there is no target as well as in the presence of a target whose location is known. While the former gives the value of f_k , the latter helps in obtaining the value of p_k . Also FLS scans in the presence of the target needs to be obtained at different ranges from the target. As mentioned in Sect. 3.1, the plot of p_k vs f_k (parametrized by t_k) is the receiver operating characteristic (ROC) curve. This ROC curve varies with signal-to-noise ratio (SNR) and environmental characteristics.

At Pandan reservoir, the ROC plots obtained matched that of detection of targets giving constant amplitude returns in Gaussian noise with an appropriate SNR (Richards 2005) at operational values of f_k (0.02–0.04) as shown in Fig. 11a. The model for this case is as follows:

$$p_k = \frac{1}{2} \operatorname{erfc} \left\{ \operatorname{erfc}^{-1}(2f_k) - \sqrt{\frac{\operatorname{SNR}}{2}} \right\} \quad (24)$$

where SNR is the signal to noise ratio, **erfc** is the complementary error function. A similar model for detection of constant amplitude targets in background noise described by stable distributions can be obtained by replacing the **erfc** function with the corresponding Q -function (**erfc** function is related to the Q -function as $2Q(\sqrt{2}x) = \operatorname{erfc}(x)$) of a “standard” stable distribution. Stable distributions are parameterized by the *characteristic exponent* α ($0 < \alpha \leq 2$), *skew parameter* β ($-1 \leq \beta \leq 1$), *location* μ ($\mu \in \mathbb{R}$) and *scale parameter* γ ($\gamma > 0$). Also, stable distributions do not have a general closed form probability density function (pdf) $g_{\alpha,\beta}(x; \gamma, \mu)$ except for special cases where $\alpha = 1$ (Cauchy distribution) or $\alpha = 2$ (Gaussian distribution). Since we are replacing the **erfc** function with the corresponding Q -function of a “standard” stable distribution, the values of μ and γ are set to 0 and $\frac{1}{\sqrt{2}}$ respectively. It should be noted that in literature, the value of γ for a standard stable distribution is usually set to 1. But the **erfc** function is with respect to a standard normal (or Gaussian) distribution where the variance, $\sigma^2 = 1$ and since $\sigma^2 = 2\gamma^2$ (when $\alpha = 2$), we get $\gamma = 1/\sqrt{2}$. The model so obtained is as follows (refer to Appendix 1 for derivation):

Fig. 9 Distribution of background noise at Pandan reservoir. **a** Range bin 15. **b** Range bin 20. **c** Range bin 25. **d** Range bin 28

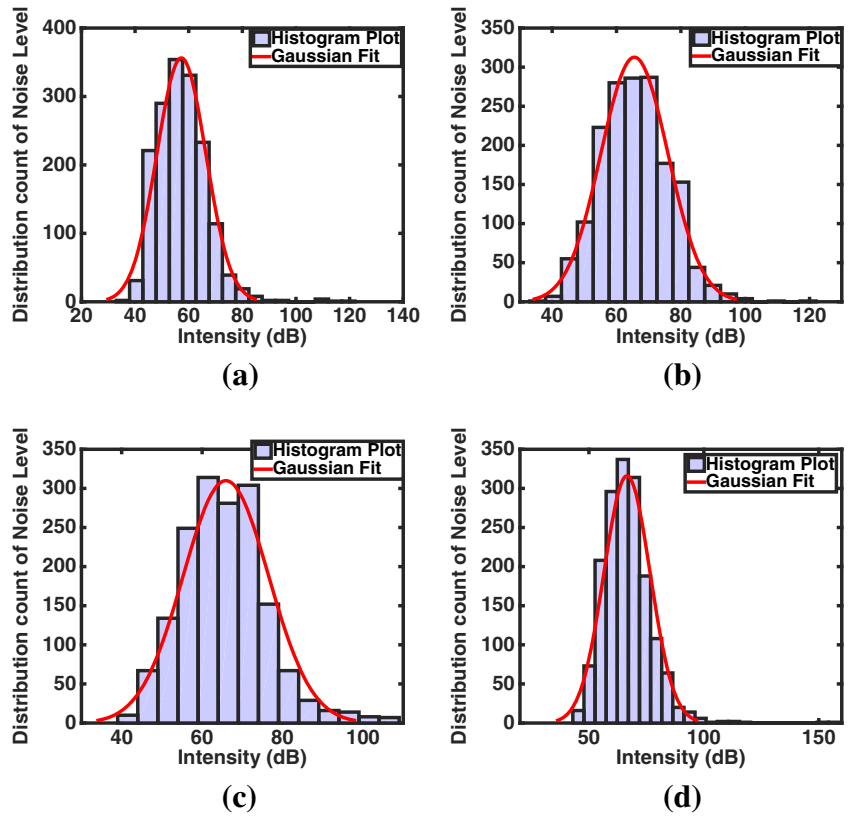
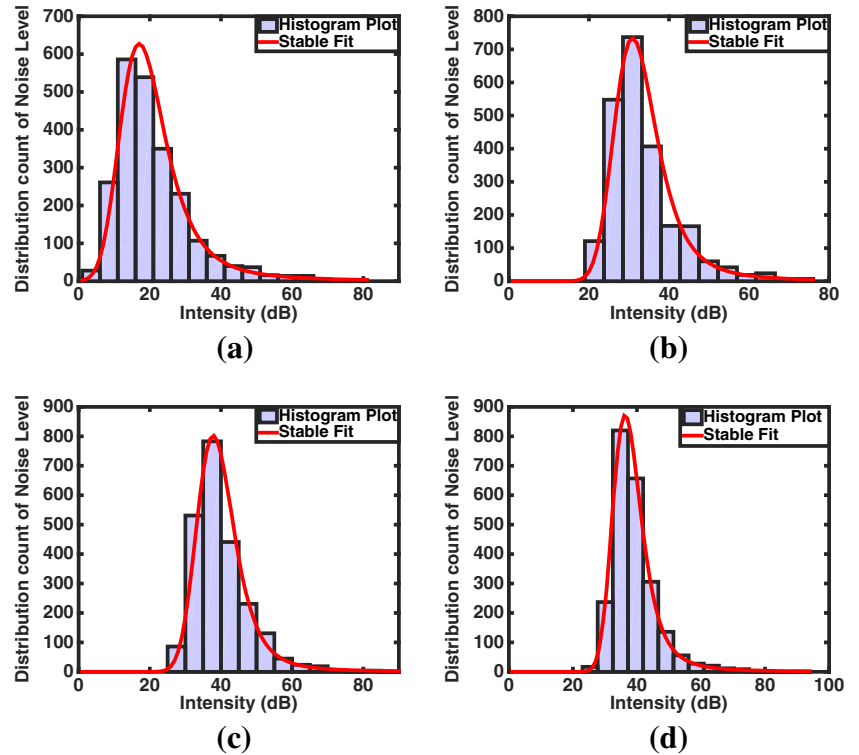


Fig. 10 Distribution of background noise at Selat Pauh. **a** Range bin 20. **b** Range bin 26. **c** Range bin 33. **d** Range bin 40



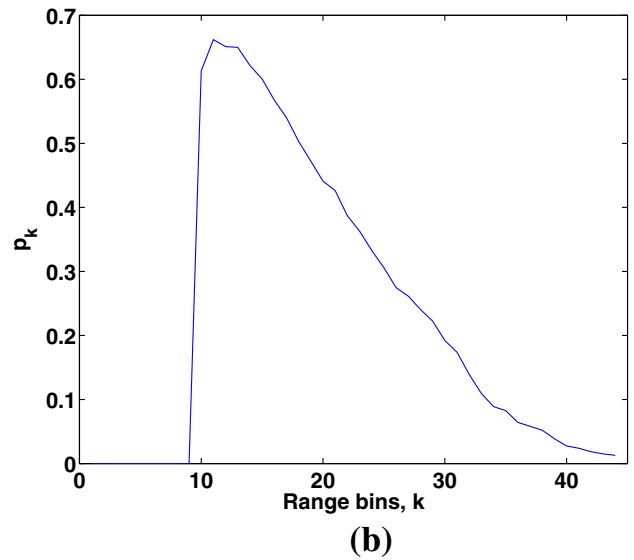
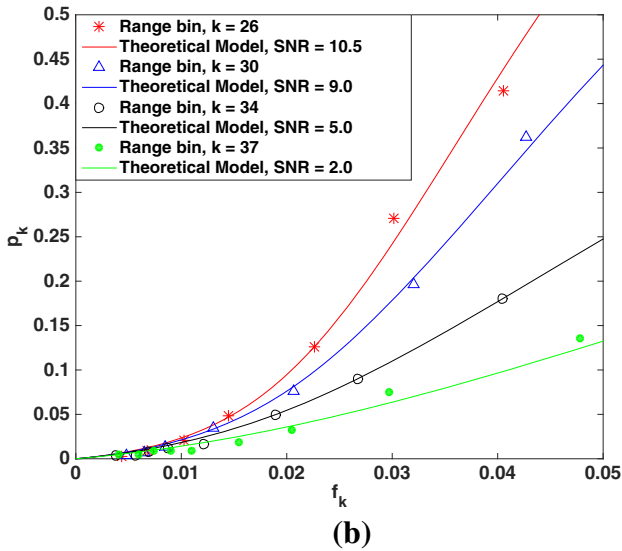
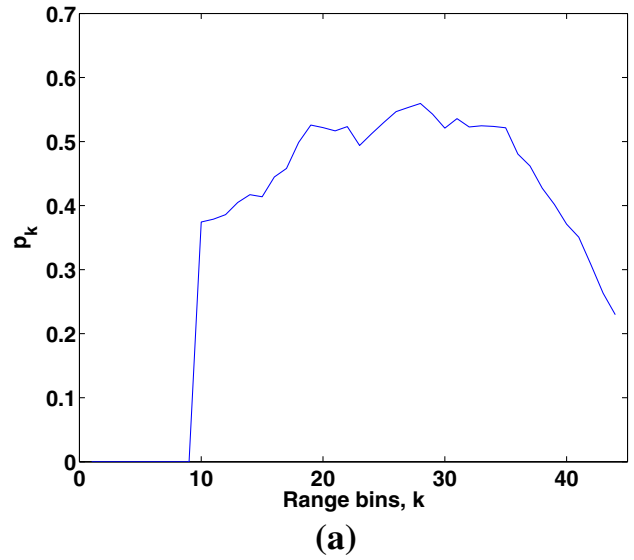
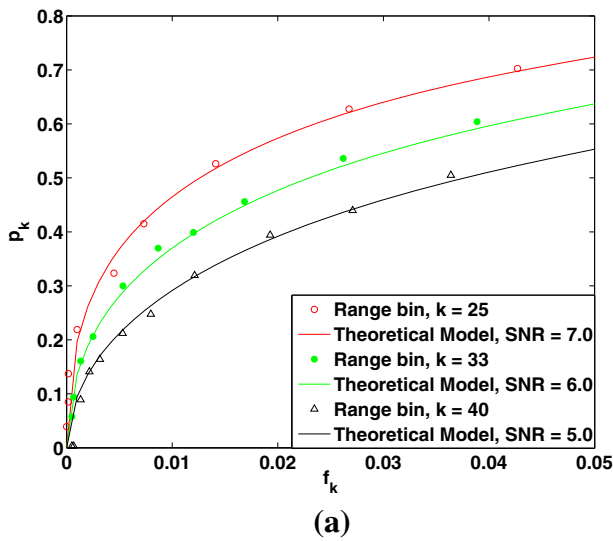


Fig. 11 Experimentally obtained ROC plots. **a** ROC plot at Pandan reservoir and the corresponding theoretical curves. **b** ROC plot at Selat Pauh and the corresponding theoretical curves

Fig. 12 Experimentally obtained operational p_k vs range bins, k . **a** Pandan reservoir, $f = 0.02$. **b** Selat Pauh, $f = 0.03$

$$p_k = Q_{\alpha_k, \beta_k} \left\{ Q_{\alpha_k, \beta_k}^{-1}(f_k) - \sqrt{SNR} \right\} \quad (25)$$

$$Q_{\alpha_k, \beta_k}(x) = \int_x^\infty g_{\alpha_k, \beta_k} \left(t; \frac{1}{\sqrt{2}}, 0 \right) dt \quad (26)$$

It should be noted that the values of α_k can be obtained from the stable fit of the background noise for the corresponding range bin, k . Also, since all the stable fits are right skewed, we can set $\beta_k = 1$ for all range bins. Finally, the ROC plots obtained experimentally matched the model for detection of targets giving constant amplitude returns in impulsive noise described by stable distributions (Eq. 25) as shown in Fig 11b.

The operational values of f_k (0.02-0.04) are suggested in the literature of detection theory using sonars (Brekke et al. 2010, 2011). At Pandan reservoir, we set the desired false alarm rate $f = 0.02$ and obtained the corresponding p_k and t_k values from the ROC curves for all range bins. Plot of p_k vs range bins for the experiment at Pandan reservoir is shown in Fig. 12a.

As the sea was much noisier than the reservoir, we set a slightly higher rate of false alarm $f = 0.03$ to ensure good detections. Plot of p_k vs range bins for the experiment at Selat Pauh is shown in Fig. 12b. It should be noted that the p_k for the first 9 range bins are zero. It is because this region is the blind zone of the sonar and any non zero intensity values received in these range bins should be discarded as well.

4.1.2 Scan results

The scans from the FLS were processed online and local occupancy grids were generated. Obstacles such as the reservoir embankments, buoys and coral reefs were clearly detected as shown in Figs. 13, 14 and 15.

From the unprocessed sonar scans shown in Figs. 13, 14 and 15 (left column), we see that the targets cannot always be clearly distinguished from the background noise. Multiple scans are processed and assimilated into the local occupancy grid as the AUV moves. The results from this process are seen in Figs. 13, 14 and 15 (middle column). It can be observed

that the cells corresponding to obstacles have a high probability of occupancy. The improvement comes from combining information from multiple scans. The Bayesian update effectively weighs the information from multiple scans based on its reliability. Figure 15 shows how reliably a small target (buoy) can be consistently detected and tracked during the course of a mission.

Finally, a hard-decision detection procedure is used at the end of each scan to detect potential obstacles. The P_{thresh} value discussed in Sect. 3.3 was set at 0.8. Obstacles such as buoys, reservoir embankments and coral reefs are detected reliably as shown in Figs. 13, 14 and 15 (right column).

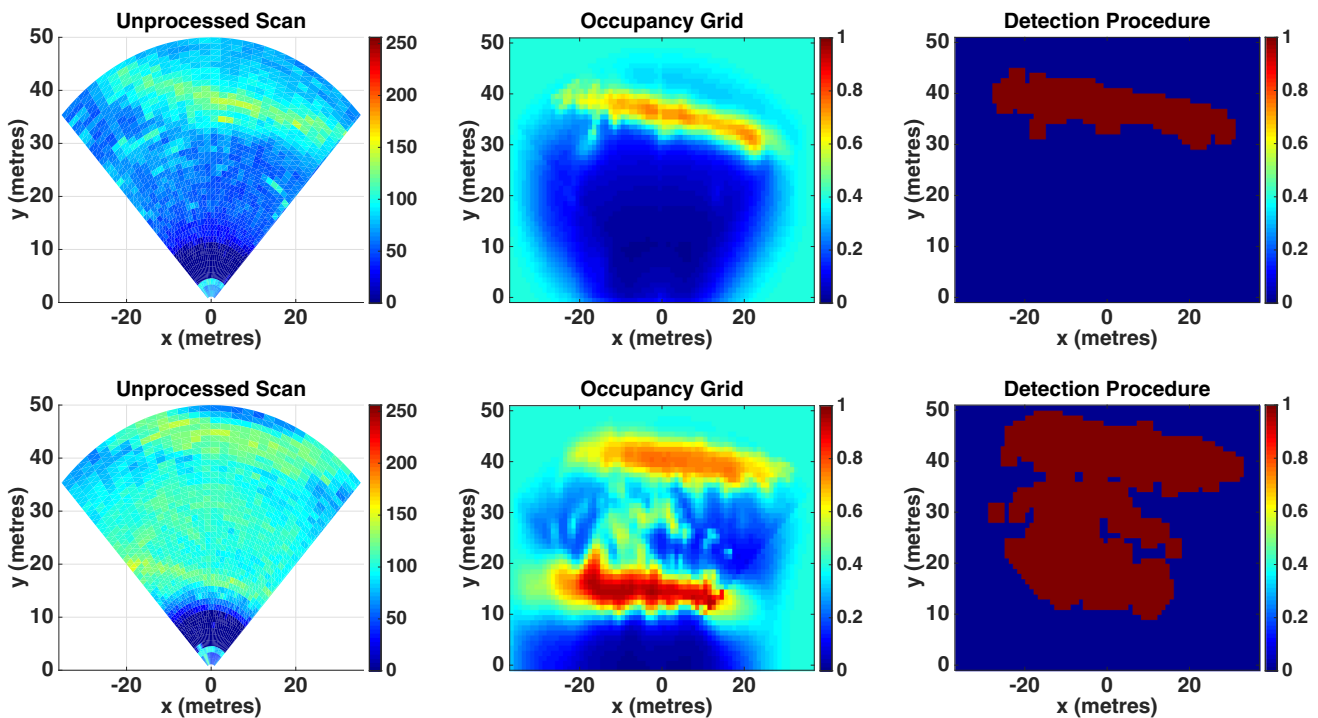


Fig. 13 Unprocessed scans (left column), occupancy grid (middle column) and obstacle detection (right column) of the reservoir's embankments during the Pandan experiment

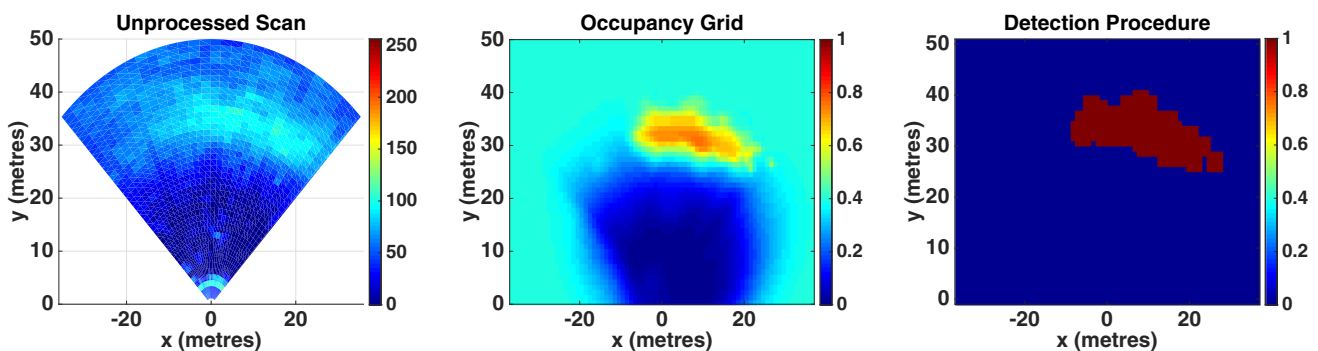


Fig. 14 Unprocessed scans (left column), occupancy grid (middle column) and obstacle detection (right column) of the coral reef during the sea experiment

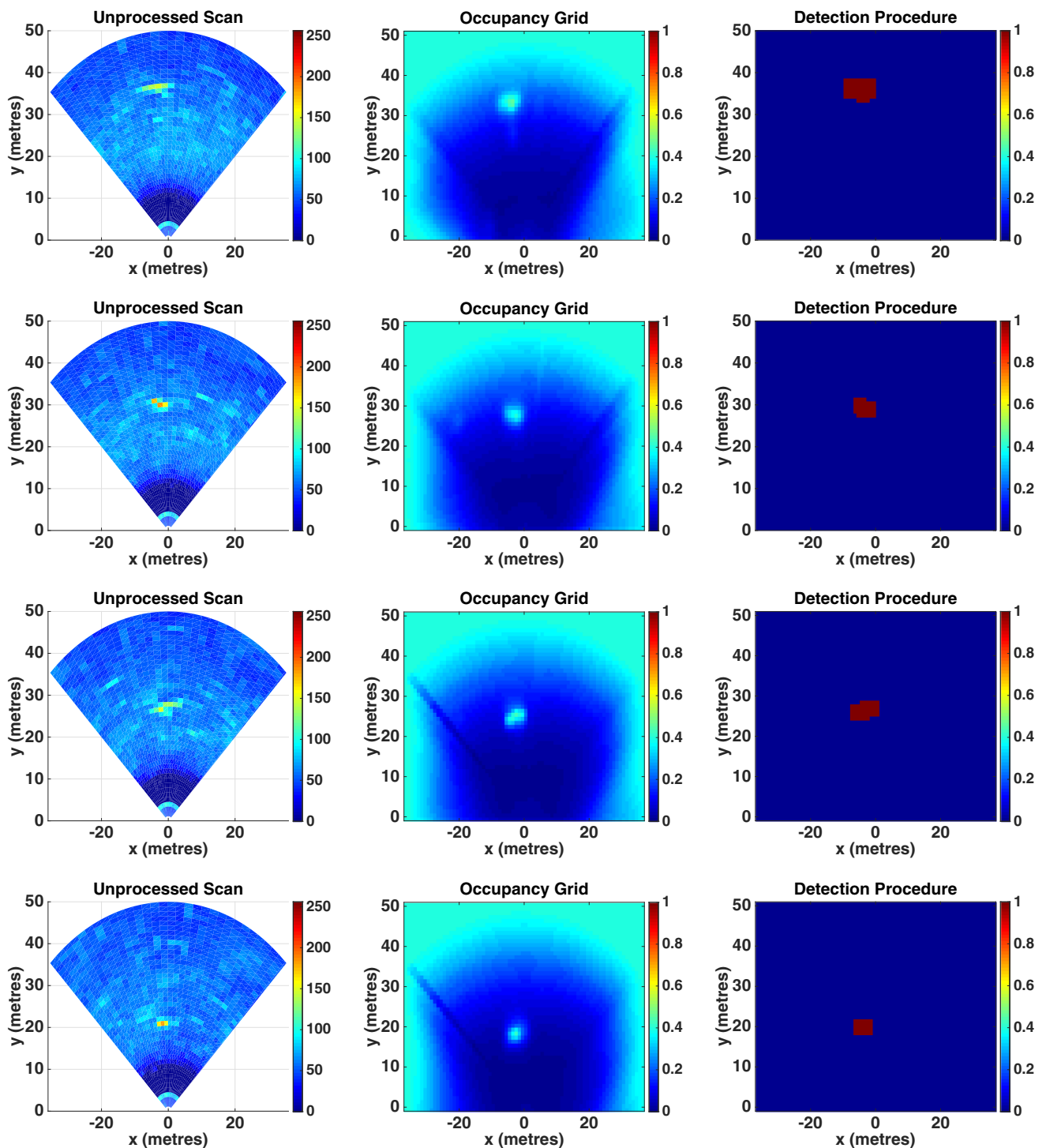


Fig. 15 Unprocessed scans (*left column*), occupancy grid (*middle column*) and obstacle detection (*right column*) of a buoy during the experiment at Pandan reservoir

4.2 Obstacle avoidance

Experiments to demonstrate the avoidance capability of the AUV were conducted at Pandan reservoir in Singapore. We used a Micron DST sector scanning sonar integrated on our

STARFISH AUV (Koay et al. 2011). Two missions were planned such that two separate buoys present themselves as obstacles when the AUV runs the mission. The locations of the buoys were noted and the missions were planned as shown in Fig. 16.

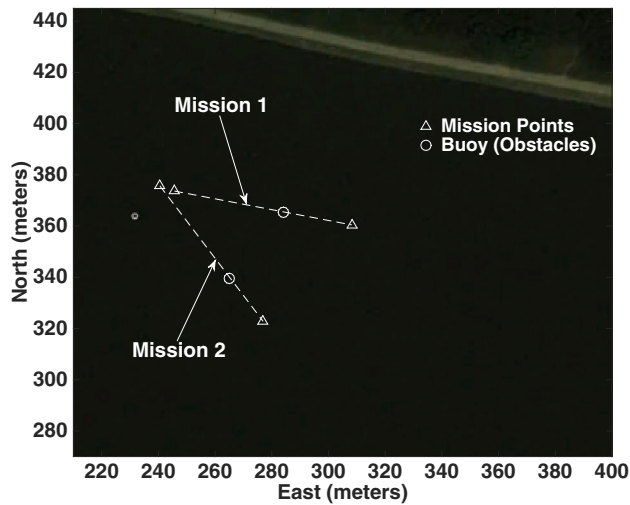


Fig. 16 Missions planned at Pandan Reservoir

During both the missions, the AUV was operating at a depth of 0.5 m and the sonar was configured to 50 m operating range. The buoys were 75 % percent submerged and 25 % above the water level. The buoys were cylindrical, with a diameter of 15 cm and a length of 70 cm, and were hemispherical at both ends. A similar buoy is shown in Fig. 17a. An illustration of the setup of the buoy at Pandan reservoir is shown in Fig. 17b.

The buoys were clearly detected in both the missions. During the second mission, the Navigator re-planned as soon as the obstacle was detected since the Navigator anticipated a collision. However, during the first mission, the buoy was detected much earlier but did not lie within the AUV's pre-planned path. This can be seen in Fig. 18. Figure 19 shows the obstacle maps and the re-planned waypoints in the AUV's frame of reference.

Once the Navigator has planned a new set of waypoints, they are sent to the Pilot of the AUV via the Executive Officer. The Pilot then carries out the appropriate avoidance maneuver. Figure 20 shows the path taken by the AUV and the re-planned waypoints in the global frame of reference. It can be seen that in both the missions, the obstacles (buoys) were avoided comfortably without posing any threat to the safety of the AUV.

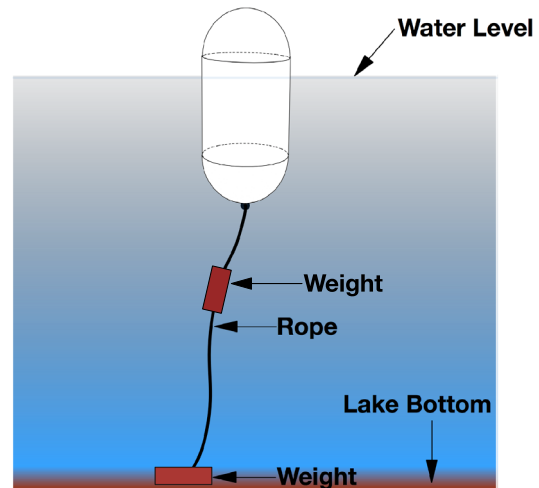
5 Discussion

5.1 Complexity analysis

Our proposed approach is computation less intensive as compared to SLAM techniques. This is because the complexity of our approach varies linearly with the number of the occupancy cells T ($= m \times n$) and the number of range bins



(a)



(b)

Fig. 17 Obstacle (buoy) to be avoided at Pandan Reservoir. a Atypical buoy. b Illustration of the buoy at Pandan Reservoir

K , i.e., $O(TK)$. Since these parameters are fixed, the complexity of the approach does not vary during the course of a mission. In other words, our approach has a constant complexity.

On the other hand, SLAM techniques usually have variable complexities. The EKF-based SLAM (Motarlier and Chatila 1989) has a complexity of $O(N^2)$, where N is the number of landmarks. The authors in Leedekerken et al. (2006) have managed to place a bound on the complexity by using local submaps. By doing so, they sacrifice the accuracy of the global map which is not desirable. Power-SLAM (Nerurkar and Roumeliotis 2007), which is also an EKF-based SLAM approach manages to reduce the complexity to $O(N)$ by applying suitable approximations. Particle filter based approaches to SLAM have also been explored in

Fig. 18 Collision checking by the Navigator during Mission 1. **a** 5 scans prior to re-planning. **b** 2 scans prior to re-planning

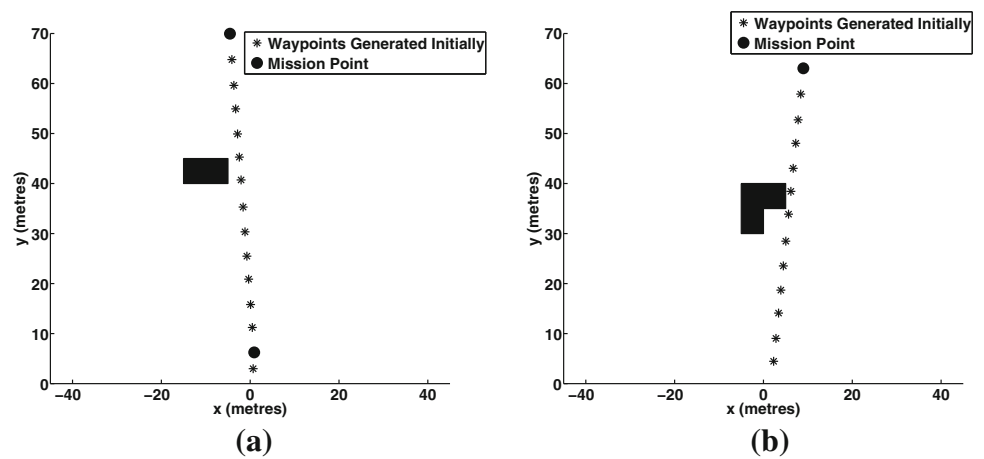


Fig. 19 Waypoint re-planning by the Navigator. **a** Mission 1. **b** Mission 2

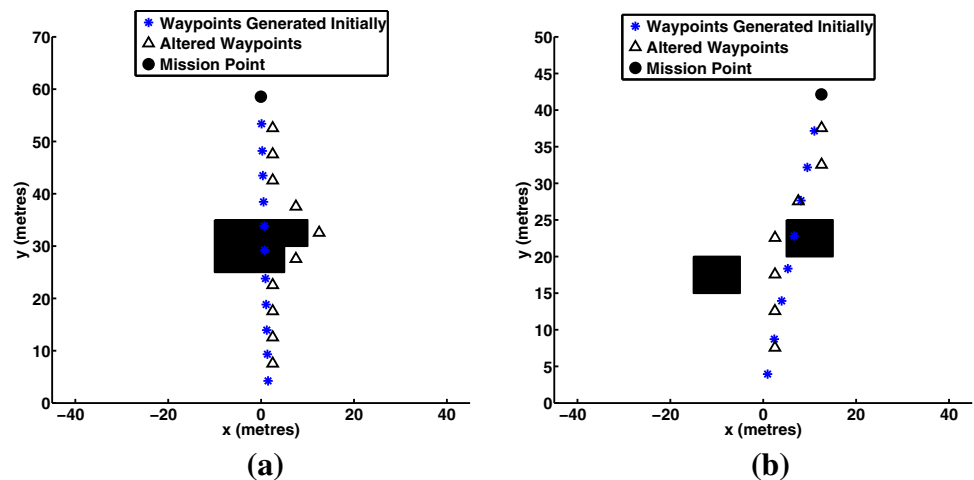
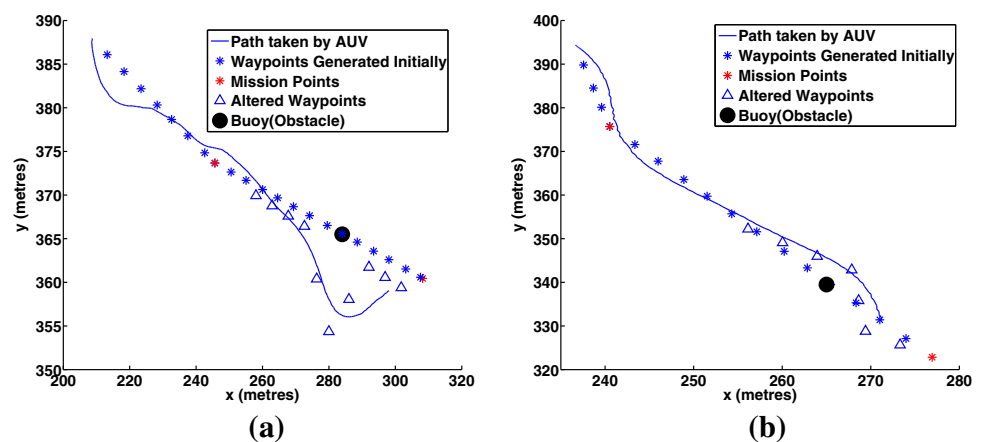


Fig. 20 Experimental Results of Obstacle Avoidance at Pandan Reservoir. **a** Mission 1. **b** Mission 2



the form of FastSLAM (Montemerlo and Thrun 2003) which has a complexity in the order of $O(M \log(N))$, where M is the number of particles and N is the number of landmarks. Another popular particle filter based SLAM is the Dynamic Particle-SLAM (DP-SLAM) (Eliazar and Parr 2004) which has a complexity of $O(MA)$, where M is the number of particles and A is the area swept by the laser. Although only the

complexities of a few major SLAM techniques have been discussed above, it is reasonable to expect variable complexities from other SLAM techniques as well. A review of the state of the art underwater slam techniques has been discussed in Hidalgo and Braunl (2015).

Since SLAM techniques solve an entirely different problem of improving positional accuracy and building accurate

global maps, it is not really fair to compare the complexities of SLAM techniques against our approach. However, from the point of view of obstacle detection and avoidance alone, if one were to compare using SLAM techniques to improve the positioning accuracy and hence estimate the position of the obstacle in a global frame to carry out an avoidance maneuver as opposed to our approach, then our approach can be seen to be computationally less intensive as it has a constant complexity.

5.2 Detection and avoidance analysis

From Sect. 4.1.1, it can be seen that the theoretical model for detection of targets giving constant amplitude returns in Gaussian noise has been validated with experimental data. We derived a theoretical model for detection in impulsive noise (described by a stable distribution) and also validated the same with experimental data.

After setting the false alarm rate f , we obtain the operating p_k and t_k for the experiments at Pandan reservoir and Selat Pauh. The choice of f and hence p_k and t_k yields very high probabilities of occupancy for obstacles like lake wall and reef. In addition to that, weak targets like buoys are detected consistently. Given the limitation of the sonar being used which has a fan shaped beam (3° (horizontal) \times 40° (vertical)), it is difficult to ensure that the detected obstacle is on the plane of navigation. In order to be safe, we treat all obstacles detected to be in the same plane of navigation and if they pose a threat of collision, we execute an avoidance maneuver.

Furthermore, for the experiments in Pandan reservoirs, the missions were executed at an altitude of 2–4 m. At this altitude, we expect considerable amount of returns from the lake bottom and this can be seen in the raw scans in Figs. 13 and 15. Our algorithm was able to accurately filter out reflections from the lake bottom and detect obstacles accurately. This can be attributed to the inclusion of sensor parameters t_k , f and p_k into the Bayesian framework and the choice of appropriate values for the same.

From the experiments held at Pandan reservoir, buoys were clearly detected and avoided comfortably. In Fig. 19b, another obstacle apart from the buoy (left of the buoy) was detected. However, there was no real obstacle in the reservoir. The detected obstacle was instead a spurious return. The robustness of the algorithm lies in successfully discarding these spurious returns over subsequent scans. Since spurious returns do not appear consistently from scan to scan, our algorithm can successfully lower the probability of occupancy in the subsequent scans. Finally, the detection procedure rejects these fictitious obstacles.

The proposed Bayesian framework to obstacle detection using a local occupancy grid in combination with the local re-planning strategy to execute avoidance maneuvers has the

potential to be used for long term autonomous underwater missions without having to jeopardize the safety of the AUV. Furthermore, the proposed approach does not rely on the use of expensive sensors for reliable obstacle detection and accurate localization of the AUV itself.

6 Conclusions and future work

We developed a novel method for underwater obstacle detection using a probabilistic local occupancy grid. We demonstrated its capability to detect obstacles robustly, avoid them and deal with noisy data by using a probabilistic framework. Given the practical limitation of the sonar being used, spurious returns cannot be eliminated in one scan and require subsequent scans to lower the probability of occupancy and finally void the detection. Our approach deals also directly with positional uncertainty by adopting an occupancy grid in the AUV's frame of reference. Hence, the obstacles are accurately localized relative to the AUV. By using occupancy grids, we addressed the problem of reliable feature extraction in underwater environments.

Furthermore, as explained in Sect. 5, our approach is computationally less intensive as compared to using SLAM based approaches for obstacle detection and avoidance. In contrast to the image processing techniques mentioned earlier which make use of heuristic approaches like segmentation to detect obstacles, a more formal approach to sonar detection is adopted. This can be seen from the validation of theoretical models of detection using experimental data (Sect. 4.1.1) following which suitable parameters for detection (f , t_k and p_k) are chosen.

However, the AUV “forgets” obstacles that it might have seen during a previous visit to a given area due to the local nature of the occupancy grid being used. Since revisiting areas is not common during most AUV missions, and considering that obstacles can be reliably re-detected, we do not see this as a significant shortcoming. But during missions that involve a lawnmower pattern, the AUV is likely to come across previously seen obstacles. Hence, tackling this problem of the “forgetting” nature of the local occupancy grid would definitely be an improvement to the work presented.

While our work deals with detection and avoidance of mainly static targets, it does provide a natural extension for detection and tracking of dynamic targets. In particular, the motion model needs to be extended to accurately predict moving targets. The problem is particularly challenging while using a sector scanning sonar since there is a considerable delay before we get another return from the moving target. Therefore, issues such as estimation and data

association would have to be addressed in a more robust manner.

Finally, as mentioned in Sect. 3.2.1, our occupancy grid formulation makes use of the assumption of independence between occupancy cells as a convenience and not as a means to avoid the intractable computations caused by assumptions of dependency. Hence, future work would also involve developing dependency models between occupancy cells and incorporating them in the formulation.

Acknowledgments The authors would like to thank Yew Teck Tan, Bharath Kalyan and Koay Teong Beng for their valuable suggestions and immense support during the field experiments at Pandan reservoir and at Selat Pauh.

Appendix 1: Derivation of model for detection in impulsive noise

Equation (24) describes the model for calculating the ROC curves for detection of targets giving constant amplitude returns in Gaussian noise. By replacing the **erfc** function with the corresponding Q -function for a “standard” stable distribution (which describes impulsive noise), the desired model can be obtained. The choice of representing the model with a Q -function can be attributed to the fact that the cumulative distribution function, $F_{\alpha,\beta}(x; \gamma, \mu) (= 1 - Q_{\alpha,\beta}(x; \gamma, \mu))$ can be evaluated based on efficient numerical approximations Nolan (1997). The derivation is as follows:

$$\text{erfc}(x) = 2Q(\sqrt{2}x) \quad (27)$$

$$Q^{-1}(x) = \sqrt{2}\text{erf}^{-1}(1 - 2x) \quad (28)$$

$$\text{erfc}^{-1}(x) = \text{erf}^{-1}(1 - z) \quad (29)$$

Substituting Eqs. (27), (28) and (29) in Eq. (24), we get:

$$xp_k = Q\{Q^{-1}(f_k) - \sqrt{SNR}\} \quad (30)$$

and replacing the Q -function with the corresponding Q -function of a stable distribution, Eq. 30 becomes:

$$p_k = Q_{\alpha_k, \beta_k} \left\{ \left(Q_{\alpha_k, \beta_k}^{-1}(f_k; \gamma, \mu) - \sqrt{SNR} \right); \gamma, \mu \right\} \quad (31)$$

The choice of values for α_k , β_k , γ , and μ for a “standard” stable distribution have been explained in Sect. 4.1.1.

Appendix 2: Justification of decoupling translational motion and rotational motion

During a mission, both translational motion and rotational motion happen simultaneously. Decoupling them is an

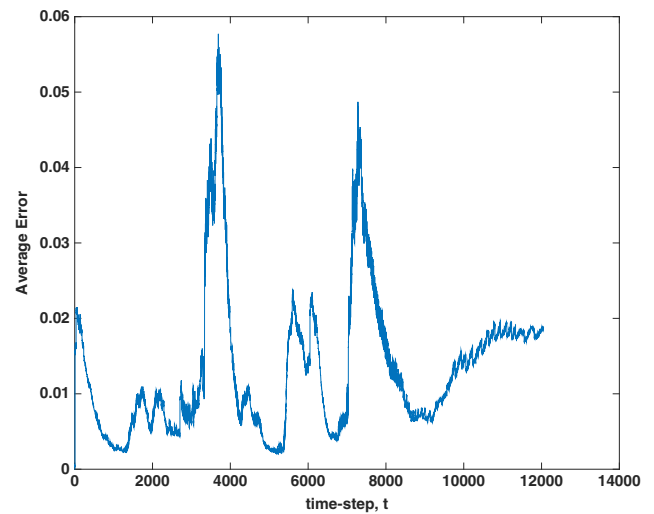


Fig. 21 Average error, ϵ_t vs time-step, t

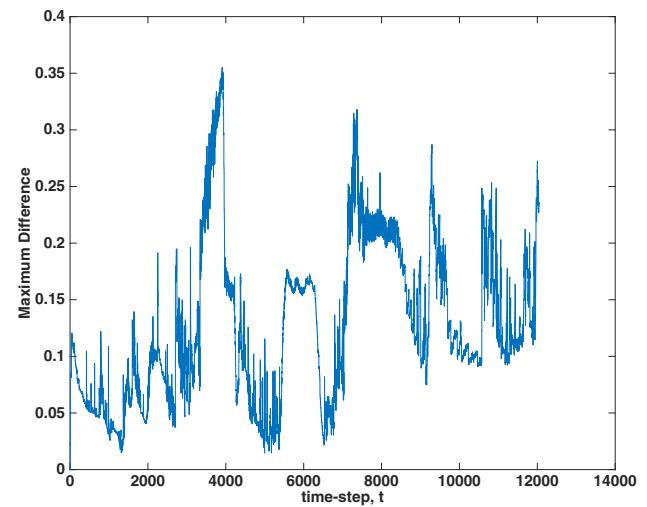


Fig. 22 Maximum difference, δ_t vs time-step, t

approximation to allow for real time performance of the algorithm. The computational intensity arises from the fact that at every time-step, the overlap of the occupancy cells that undergoes both translation and rotation, with the occupancy cells prior to translation and rotation, needs to be calculated. In other words, the values of $w_{x,y}^{x-i,y-j}$ in Eq. (21) need to be calculated at every time-step in order to update the occupancy grid using Eq. (21). Note that for this case, the values of $w_{x,y}^{x-i,y-j}$ account for both translational and rotational motion. To justify the approximation, we calculated the actual values of $w_{x,y}^{x-i,y-j}$ offline and use them to update the occupancy grid (Eq. 21). Figure 21 shows how the average error throughout the grids varies with time (for the mission at Pandan reservoir) and is calculated as follows:

$$\epsilon_t = \frac{1}{mn} \left| \sum_{i=1}^m \sum_{j=1}^n P(O_{i,j})_t'' - \sum_{i=1}^m \sum_{j=1}^n P(O_{i,j})_t \right| \quad (32)$$

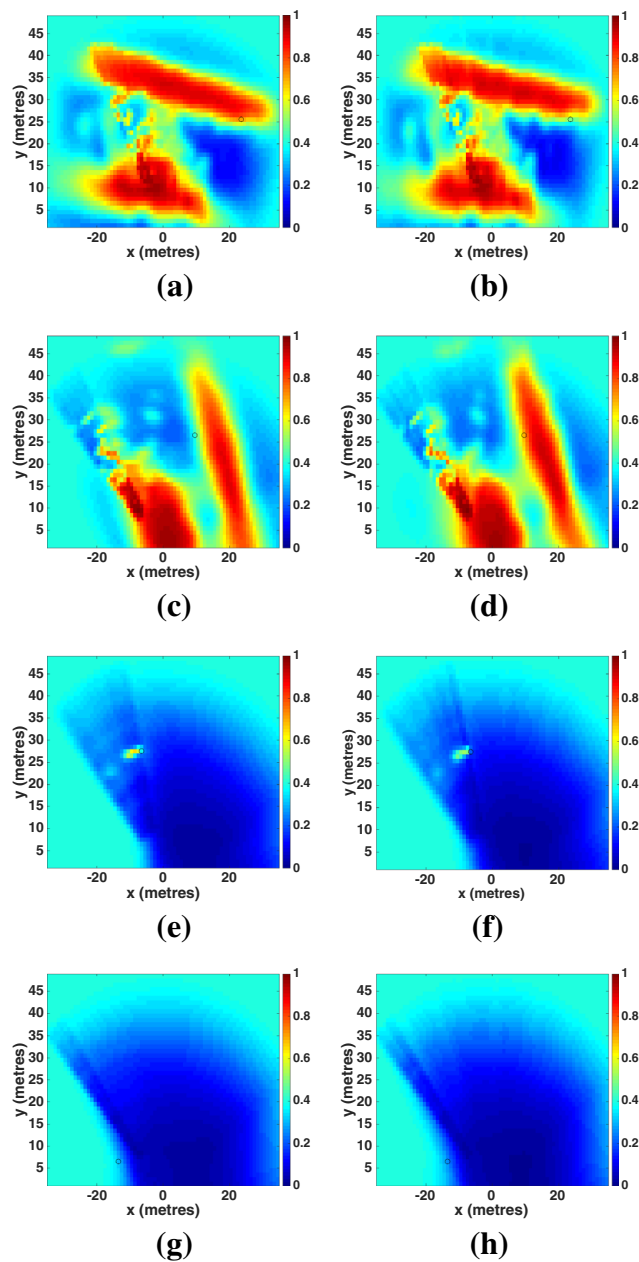


Fig. 23 Occupancy grids at different time-steps. **a, c, e, g** Benchmark. **b, d, f, h** Approximation

where $P(O_{i,j})'_t$ and $P(O_{i,j})_t$ are the probabilities of occupancy calculated according to the benchmark model and approximated model respectively at time-step t . It can be seen that the maximum average error is only of the order of 0.058 which is certainly not a cause for concern. Also, we see the average error increasing and decreasing between time-steps 3000–4000, 5500–6500, and 7000–9000. This can be explained by the fact that the AUV is undergoing rotational motion during these time intervals and since the approximation is done on the rotational motion, we see an increase in the average error.

Furthermore, we calculate the maximum difference (Eq. 33) between the probabilities of occupancy estimated according to the two models at every time-step (Fig. 22).

$$\delta_t = \max\{P(O_{i,j})'_t - P(O_{i,j})_t\}; \forall i \in \{1, \dots, m\}, j \in \{1, \dots, n\} \quad (33)$$

Again, the maximum difference is increasing and decreasing between the same time-steps mentioned above. But, the values of the maximum difference between the probabilities during these intervals are quite high (0.15–0.35). This can be explained by the fact that the benchmark model takes the rotational motion of the AUV into account at every time-step as opposed to the approximated model where the changes in heading are allowed to accumulate till $\pm 1^\circ$. As a result, the detected obstacles are “shifted” (rotated) regularly in the benchmark model while they are “shifted” (rotated) only when there is a $\pm 1^\circ$ change in heading. Therefore, we can expect the occupancy cells contributing to the maximum difference between the probabilities of occupancy to be at the boundary region of a detected obstacle. In the event that there is no obstacle, the maximum difference is likely to occur at the boundary of the “sector scan”. This is justified in the various scans shown in Fig. 23.

The black circle on the occupancy grids in Fig. 23 indicates the the occupancy cells that contribute to the maximum difference between the probabilities of occupancy calculated using the benchmark and approximated model. It can clearly be seen that the occupancy cells at the boundary of the obstacle are the ones contributing to the maximum difference in probabilities. Furthermore, in the approximation, the occupancy cell (black circle) is only one or two cells away from the actual boundary. The radius of clearance, o cells, defined for obstacle avoidance (Sect. 3.4.2) is always greater than two cells (usually set to five cells). Hence, from the point of view of executing an avoidance maneuver which is the motive of the paper, this approximation can be justified.

References

- Brekke, E., & Chitre, M. (2013). Bayesian Multi-Hypothesis Scan Matching. *Proceedings of OCEANS'13* (pp. 1–10). Norway: Bergen.
- Brekke, E., Hallingstad, O., & Glattetre, J. (2010). The signal-to-noise ratio of human divers. In *OCEANS 2010 IEEE—Sydney* (pp. 1–10).
- Brekke, E., Hallingstad, O., & Glattetre, J. (2011). The modified riccati equation for amplitude-aided target tracking in heavy-tailed clutter. *IEEE Transactions on Aerospace and Electronic Systems*, 47(4), 2874–2886.
- Burguera, A., González, Y., & Oliver, G. (2012). The UspIC: Performing scan matching localization using an imaging sonar. *Sensors*, 12(6), 7855–7885.

- Castellanos, J. A., Martínez-Cantin, R., Tardós, J. D., & Neira, J. (2007). Robocentric map joining: Improving the consistency of ekf-slam. *Robotics and Autonomous Systems*, 55(1), 21–29.
- Chew, J. L., & Chitre, M. (2013). Object detection with sector scanning sonar. In *Proceedings of OCEANS'13* (pp. 1–8), San Diego.
- Chitre, M., Potter, J., & Ong, S. H. (2006). Optimal and near-optimal signal detection in snapping shrimp dominated ambient noise. *IEEE Journal of Oceanic Engineering*, 31(2), 497–503.
- Elfes, A. (1989). Using occupancy grids for mobile robot perception and navigation. *Computer*, 22(6), 46–57.
- Eliazar, A. (2005). DP-SLAM. PhD thesis, Department of Computer Science, Duke University, Durham.
- Eliazar, A., & Parr, R. (2004). DP-SLAM 2.0. In *IEEE International Conference on Robotics and Automation, ICRA '04* (vol 2, pp 1314–1320).
- Fairfield, N., Kantor, G., & Wettergreen, D. (2007). Real-time slam with octree evidence grids for exploration in underwater tunnels. *Journal of Field Robotics*, 24(1–2), 03–21.
- Fulgenzi, C., Spalanzani, A., & Laugier, C. (2007). Dynamic obstacle avoidance in uncertain environment combining pvos and occupancy grid. In *IEEE International Conference on Robotics and Automation* (pp. 1610–1616).
- Hart, P., Nilsson, N., & Raphael, B. (1968). A formal basis for the heuristic determination of minimum cost paths. *IEEE Transactions on Systems Science and Cybernetics*, 4(2), 100–107.
- Hernández, E., Ridao, P., Mallios, A., & Carreras, M. (2009). Occupancy grid mapping in an underwater structured environment. In *IFAC Proceedings Volumes (IFAC-PapersOnline)* (pp. 286–291).
- Hidalgo, F., & Braunl, T. (2015). Review of underwater slam techniques. In *International Conference on Automation, Robotics and Applications* (pp. 306–311).
- Horner, D., McChesney, N., Masek, T., & Kragelund, S. (2009). 3D reconstruction with an AUV mounted forward-looking sonar reconstruction with an auv mounted forward-looking sonar. In *Proceedings of International Symposium on Unmanned Untethered Submersible Technology* (pp. 1464–1470).
- Horner, D. P., Healey, A. J., & Kragelund, S. P. (2005). AUV experiments in Obstacle Avoidance. *Proceedings of MTS/IEEE OCEANS*, 2, 1464–1470.
- Hurtós, N., Ribas, D., Cufí, X., Petillot, Y., & Salvi, J. (2015). Fourier-based registration for robust forward-looking sonar mosaicing in low-visibility underwater environments. *Journal of Field Robotics*, 32(1), 123–151.
- Jakuba, M., & Yoerger, D. (2008). Autonomous search for hydrothermal vent fields with occupancy grid maps. In *Proceedings of the 2008 Australasian Conference on Robotics and Automation, ACRA 2008*.
- Koay, T., Tan, Y., Eng, Y., Gao, R., Chitre, M., Chew, J., et al. (2011). STARFISH-A small team of autonomous robotic fish. *Indian Journal of Geo-Marine Sciences*, 40(2), 157–167.
- Konolige, K. (1997). Improved occupancy grids for map building. *Autonomous Robots*, 4(4), 351–367.
- Leedekerken, J.C., Leonard, J.J., Bosse, M.C., & Balasuriya, A. (2006). Real-time obstacle avoidance and mapping for AUVs operating in complex environments. In *Proceedings of the 7th International Mine Warfare Symposium*, Monterey
- Majumder, S., Rosenblatt, J., Scheding, S., & Durrant-whyte, H. (2001). Map building and localization for underwater navigation. *Experimental Robotics VII* (Vol. 271, pp. 511–520), Lecture Notes in Control and Information Sciences, Berlin Heidelberg: Springer.
- Marlow, S.Q., & Langelaan, J.W. (2010). Dynamically sized occupancy grids for obstacle avoidance. In *AIAA Guidance, Navigation, and Control Conference*
- Martin, A., An, E., Nelson, K., & Smith, S. (2000). Obstacle detection by a forward looking sonar integrated in an autonomous underwater vehicle. In *OCEANS 2000 MTS/IEEE Conference and Exhibition* (vol. 1, pp. 337–341), Providence, RI
- Montemerlo, M., & Thrun, S. (2003). Simultaneous localization and mapping with unknown data association using fastslam. In *IEEE International Conference on Robotics and Automation, ICRA '03* (vol. 2, pp. 1985–1991).
- Motarlier, P., & Chatila, R. (1989). Stochastic multi-sensory data fusion for mobile robot location and environmental modeling. In *5th International Symposium on Robotics Research* (pp. 85–94).
- Nerurkar, E. D., & Roumeliotis, S. (2007). Power-SLAM: A linear-complexity, consistent algorithm for SLAM. *IEEE/RSJ International Conference on Intelligent Robots and Systems, IROS, 2007*, 636–643.
- Nolan, J. P. (1997). Numerical calculation of stable densities and distribution functions. *Communications in Statistics-Stochastic Models*, 13(4), 759–774.
- Quidu, I., Hetet, A., Dupas, Y., & Lefevre, S. (2007). AUV (Redermor) obstacle detection and avoidance experimental evaluation. *OCEANS 2007—Europe* (pp. 1–6). UK: Aberdeen.
- Ribas, D., Ridao, P., Tardós, J. D., & Neira, J. (2008). Underwater SLAM in man-made structured environments. *Journal of Field Robotics*, 25(11–12), 898–921.
- Richards, M. (2005). *Fundamentals of radar signal processing* (pp. 304–316). New Delhi: Tata McGraw-Hill.
- Stentz A (1994) Optimal and efficient path planning for partially-known environments. In *IEEE International Conference on Robotics and Automation, ICRA 1994* (vol. 4, pp. 3310–3317).
- Teck TY, Chitre M (2012) Hierarchical multi-agent command and control system for autonomous underwater vehicles. In *Autonomous Underwater Vehicles (AUV), 2012 IEEE/OES* (pp. 1–6).
- Teck, T. Y., & Chitre, M. (2014). Direct policy search with variable-length genetic algorithm for single beacon cooperative path planning. *Distributed Autonomous Robotic Systems*, 104, 321–336.
- Tena R. I., Petillot, Y., Lane, D., & Bell, J. (1999). Tracking objects in underwater multibeam sonar images. In *IEEE Colloquium on Motion Analysis and Tracking* (pp. 11/1–11/7).
- Teo, K., Ong, K. W., & Lai, H. C. (2009). Obstacle detection, avoidance and anti collision for MEREDITH AUV. *OCEANS 2009, MTS/IEEE Biloxi—Marine technology for our future* (pp. 1–9). Global and Local Challenges, Biloxi, MS.
- Thrun, S., Burgard, W., & Fox, D. (2005). *Probabilistic robotics (intelligent robotics and autonomous agents)*. Cambridge: MIT Press.
- Zhao, S., Lu, T. F., & Anvar, A. (2009). Automatic object detection for AUV navigation using imaging sonar within confined environments. In *4th IEEE Conference on Industrial Electronics and Applications, ICIEA 2009* (pp. 3648–3653).



Varadarajan Ganesan received his B.Eng. and M.Eng degrees in Mechanical and Electrical & Computer Engineering respectively from the National University of Singapore (NUS). His Master's thesis involved developing a robust underwater obstacle detection and avoidance system. He is current working at the Acoustic Research Laboratory (ARL), NUS, as a Research Engineer. His research interests include co-operative mobile robotics, autonomous underwater

vehicles (AUVs), terrain aided navigation, and unmanned aerial vehicles (UAVs).



Mandar Chitre received B.Eng. and M.Eng. degrees in electrical engineering from the National University of Singapore (NUS), Singapore, a M.Sc. degree in bioinformatics from the Nanyang Technological University (NTU), Singapore, and a Ph.D. degree from NUS. From 1997 to 1998, he worked with the ARL, NUS in Singapore. From 1998 to 2002, he headed the technology division of a regional telecommunications solutions company. In 2003, he rejoined ARL, initially

as the Deputy Head (Research) and is now the Head of the laboratory. Dr. Chitre also holds a joint appointment with the Department of Electrical & Computer Engineering at NUS as an Assistant Professor. His current research interests are underwater communications, autonomous underwater vehicles, model-based signal processing and modeling of complex dynamic systems. Dr. Chitre has served on the technical program committees of the IEEE OCEANS, WUWNet, DTA and OTC conferences and has served as reviewer for numerous international journals. He was the chairman of the student poster committee for IEEE OCEANS'06 in Singapore, and the chairman for the IEEE Singapore AUV Challenge 2013. He is currently the IEEE Ocean Engineering Society technology committee co-chair of underwater communication, navigation & positioning.



Edmund Brekke received the M.Sc. degree in industrial mathematics in 2005, and the Ph.D. degree in engineering cybernetics in 2010, both from the Norwegian University of Science and Technology (NTNU), Trondheim, Norway. From 2010 to 2014, he worked with the Acoustic Research Laboratory (ARL), NUS in Singapore as a postdoctoral Research Fellow. In 2014 he rejoined NTNU and the Department of Engineering Cybernetics as an Associate Professor. He is an affiliated scientist

at the Centre for Autonomous Marine Operations and Systems (AMOS), and Project Manager for the knowledge-building research project "Sensor Fusion and Collision Avoidance for Autonomous Surface Vehicles". His current research interests are primarily within sensor fusion, including target tracking, detection theory, autonomous navigation and Bayesian estimation in general.